

RESEARCH ARTICLE

β1D integrin splice variant stabilizes integrin dynamics and reduces integrin signaling by limiting paxillin recruitment

Martinho Soto-Ribeiro^{1,*}, Birgit Kastberger^{1,*}, Michael Bachmann^{1,2,*}, Latifeh Azizi^{3,4}, Kenza Fouad¹, Marie-Claude Jacquier¹, David Boettiger¹, Daniel Bouvard⁵, Martin Bastmeyer², Vesa P. Hytönen^{3,4} and Bernhard Wehrle-Haller^{1,‡}

ABSTRACT

Heterodimeric integrin receptors control cell adhesion, migration and extracellular matrix assembly. While the α integrin subunit determines extracellular ligand specificity, the β integrin chain binds to an acidic residue of the ligand, and cytoplasmic adapter protein families such as talins, kindlins and paxillin, to form mechanosensing cell matrix adhesions. Alternative splicing of the β1 integrin cytoplasmic tail creates ubiquitously expressed \$1A, and the heart and skeletal musclespecific β1D form. To study the physiological difference between these forms, we developed fluorescent β1 integrins and analyzed their dynamics, localization, and cytoplasmic adapter recruitment and effects on cell proliferation. On fibronectin, GFP-tagged β1A integrin showed dynamic exchange in peripheral focal adhesions, and long, central fibrillar adhesions. In contrast, GFP-\(\beta\)1D integrins exchanged slowly, forming immobile and short central adhesions. While adhesion recruitment of GFP- $\beta1A$ integrin was sensitive to C-terminal tail mutagenesis, GFP-β1D integrin was recruited independently of the distal NPXY motif. In addition, a P786A mutation in the proximal, talin-binding NPXY⁷⁸³ motif switched β1D to a highly dynamic integrin. In contrast, the inverse A786P mutation in \$1A integrin interfered with paxillin recruitment and proliferation. Thus, differential β1 integrin splicing controls integrin-dependent adhesion signaling, to adapt to the specific physiological needs of differentiated muscle cells.

KEY WORDS: Integrins, Isoform, Splicing, Muscle, Paxillin, Adhesion, Focal adhesions, Fibrillar adhesions, Fibronectin, FRAP, Talin1, Talin2

INTRODUCTION

Heterodimeric receptors of the integrin family play crucial roles in cell adhesion and signaling during development and tissue homeostasis in the adult. In addition to varying subunit compositions that create different ligand specificity and affinities (Humphries et al., 2006; Hynes, 2002), certain integrins show also cell-type specific and developmentally regulated splicing (Fornaro and Languino, 1997). One of the best-known examples of

¹Department of Cell Physiology and Metabolism, University of Geneva, Centre Médical Universitaire, Rue Michel-Servet 1, 1211 Geneva 4, Switzerland. ²Zoological Institute, Cell- and Neurobiology, Karlsruhe Institute of Technology (KIT), Karlsruhe, Germany. ³Faculty of Medicine and Health Technology, Tampere University, Arvo Ylpön katu 34, Fl-33520 Tampere, Finland. ⁴Finlad. ⁴Finlab Laboratories, Biokatu 4, Fl-33520 Tampere, Finland. ⁵Université Grenoble Alpes, Institute for Advanced Bioscience, INSERM U823, F-38042 Grenoble, France. *These authors contributed equally to this work

[‡]Author for correspondence (bernhard.wehrle-haller@unige.ch)

B.K., 0000-0002-2806-655X; M.B., 0000-0001-9450-3458; D.B., 0000-0002-5951-4503; V.P.H., 0000-0002-9357-1480; B.W.-H., 0000-0002-1159-1147

variants formed functional β1 integrins with differences in their dynamic incorporation into focal and fibrillar adhesions. C-terminal mutations revealed that both the distal NPXY motif and the C-terminal carboxylic acid motif were critical for recruitment of the β1A variant into cell matrix adhesions, while β1D did not require these C-terminal motifs. FRAP analysis showed dynamic remodeling of the β1A integrin in focal and fibrillar adhesions, while β1D remained immobile. By employing chimeras of integrins and IL2 receptor (Tac, also known as IL2RA) (LaFlamme et al., 1994), we confirmed specific recruitment of Tac–β1D integrin to talin2-containing, central fibrillar adhesions while Tac–β1A

integrin showed less association with talin2. Despite these

differences in integrin dynamics and adapter recruitment, the

We show that extracellularly tagged β1A or β1D integrin splice

alternative splicing of the ubiquitously expressed \$1A integrin is the specific expression of the \beta 1D integrin isoform in cardiomyocytes and differentiated myotubes of skeletal muscle (Belkin et al., 1996; van der Flier et al., 1997, 1995; Zhidkova et al., 1995). Analysis in mice revealed that the knock-in of the β1D variant affected primary myogenesis and led to embryonic lethality, while the deletion of β 1D and thus the exclusive expression of the B1A variant was well tolerated (Baudoin et al., 1998; Cachaco et al., 2003). Ectopic expression of the β1D integrin isoform in myoblasts or fibroblasts revealed enhanced adhesion, integrin activation and fibronectin binding, but also reduced cell cycle progression (Belkin and Retta, 1998; Belkin et al., 1997). Some of these phenotypes, such as enhanced cell matrix adhesion, correlated with the increased affinity of the β1D integrin peptide for talin proteins in vitro (Anthis et al., 2010; Belkin et al., 1997). The particularly high affinity of the β1D cytoplasmic tail for talin2 enabled the crystallization of the complex, and nuclear magnetic resonance (NMR) perturbation experiments showed that the membrane-proximal acidic and NPXY motifs of β 1A, β 1D and β 3 integrins bound differentially to the talin head domain (Anthis et al., 2010, 2009). With the exception of a different rod domain-specific mechanosensitivity, talin1 and talin2 induce similar integrin activation, cell spreading and focal adhesion formation (Austen et al., 2015). Therefore, and especially given the enhanced binding affinity for talin1 and talin2 (Anthis et al., 2010), it is not apparent why the β 1D integrin isoform cannot functionally replace β1A integrins, with β1A integrin knockdown resulting in embryonic mortality and developmental defects in migrating cell populations (Baudoin et al., 1998). In order to better understand how altered talin-binding affinities affect the function of different β1 integrin splice variants, we exploited extracellularly tagged fluorescent β1A and β1D integrins (Egervari et al., 2016; Leduc et al., 2013). Extracellular tagging of β1A and β1D integrin allowed us to study their dynamic behavior in living cells, the unrestricted binding of cytoplasmic adapter proteins and quantitative analysis of their recruitment into different cell matrix adhesion structures.

cell matrix adhesion force was not significantly altered between $\beta1A$ - and $\beta1D$ -transfected cell populations. However, adhesion force diminished, integrin dynamics increased and central adhesion localization was lost as a result of an isoform switching mutation in $\beta1D$ integrin (P786A). In contrast, the reverse mutation in $\beta1A$ integrin (A786P) affected paxillin recruitment, which was also absent from $\beta1D$ integrin-containing adhesions, correlating with a delay in cell spreading and reduced cell proliferation. Our data demonstrate that integrin splicing can affect integrin dynamics and enable mechanically stronger linkage while reducing integrin signaling capacity in terminally differentiated striated muscle cells.

RESULTS

Extracellular GFP tagging reveals different adhesion patterns of intracellular splice variants of β1 integrin

The use of C-terminally GFP-tagged \(\beta \) integrin receptors (\(\beta \) integrin-GFP) has allowed study of the dynamic remodeling of cell matrix adhesion sites in migrating cells, and helped our understanding of how the cytoplasmic adapters such as talins associate in order to regulate integrin affinity and mechanosensing (Ballestrem et al., 2001; Cluzel et al., 2005; Pinon et al., 2014). While this approach has been mainly used to study the recruitment of β3 integrin into focal complexes and focal adhesions, the functional role of \$1 integrin-containing integrin receptors, such as the fibronectin (FN)-binding α5β1 integrin, have been less studied with live-cell imaging probes (Caswell et al., 2007; Laukaitis et al., 2001; Parsons et al., 2008). In particular, the long-term tracking of cell-surface expressed \$1 or \$3 integrins in focal or fibrillar adhesions, respectively, has only been possible with the insertion of the fluorescent tag into the extracellular domain (Egervari et al., 2016; Leduc et al., 2013) (see Fig. 1G for a model). In addition to providing a tool for the long-term tracking of cell-surface expressed β integrins (Tsunovama et al., 2018) or integrin internalization (Huet-Calderwood et al., 2017) of such β1 integrins, this technique also allows the study in great detail of the consequences of subtle sequence differences in the cytoplasmic tails of integrins. Thus, we used this strategy to study the functional role and dynamic differences of the alternatively spliced cytoplasmic tails of the ubiquitous β1A and muscle-specific β1D integrin, within the context of the FN-binding α5β1 integrin receptor. These GFP-tagged β1 integrin splice variants were transiently expressed in C2C12 myoblasts or 3T3 fibroblasts, as well as in β1 integrin-deficient GE11 and GD25 cells and compared with C-terminally tagged β1 integrin to understand their functional association with different cytoplasmic adapter proteins, such as talins and paxillin.

Expression of C-terminally tagged B1A integrin-GFP fusion constructs in 3T3 fibroblasts (Fig. 1B,D) and C2C12 myoblasts (Fig. 3I) showed cell surface expression. However, despite plating these cells on FN-coated coverslips, these integrins showed poor recruitment into peripheral focal adhesions and central fibrillar adhesions as compared to endogenous \$1 integrin labeled with monoclonal antibody clone 9EG7, detecting the extended forms of β1 integrins (Bazzoni et al., 1995; Lenter et al., 1993; Su et al., 2016) (Fig. 1A). The reduced recruitment of the C-terminally tagged \(\beta 1 A \) integrins into adhesion structures was not due to the length of the linker domain, consisting of 5 or 30 amino acids in Fig. 1B and Fig. 1D, respectively, but potentially because the free carboxylic acid is required for interaction with kindlins (Fitzpatrick et al., 2014). To avoid a non-specific interference by the cytoplasmic GFP, we decided to incorporate GFP into the extracellular domain of the \beta 1A integrin, similar to a strategy successfully used for *Drosophila* β integrin. In these animals, the

insertion of an epitope tag or fluorescent protein into a 41-aminoacid-long, serine-rich extracellular loop located in the hybrid domain was well tolerated (Bunch et al., 2006; Kendall et al., 2011; Sved et al., 2016). Although shorter in human \(\beta \) integrin, the same loop, which is localized at proline 88 (P88), offered an extracellular tagging site (Fig. 1G), which would (i) not interfere with the folding of the different structural domains of the \beta1 integrin, and (ii) would permit α integrin association and FN ligand binding (Egervari et al., 2016). Thus, transient expression of P88 loop-tagged β1A and β1D constructs allowed detection of α5β1A integrin in focal and fibrillar adhesions (Fig. 1C) and of α5β1D integrin in many small centrally located adhesion sites (Fig. 1F). Interestingly, the C-terminal tagging of the β1D splice variant (Fig. 1E) produced an identical integrin pattern to that produced by P88 loop-tagged GFP-β1D (Fig. 1F), with many short centrally located adhesions. Thus, while the \$1A splice variant showed poor functionality when modified with a C-terminal GFP tag, the β1D splice variant constructs displayed similar behavior, irrespective of the tag location.

The different patterns and organization of integrin adhesion sites seen with the extracellularly tagged β1 integrins could reflect functional differences in the alternatively spliced cytoplasmic tails. To corroborate this notion, we expressed the P88-loop-tagged GFP-\beta1A integrin and GFP-β1D integrin also in C2C12 myoblasts, and plated them on FN (Fig. 1H,I), as well as on laminin-111 (Fig. 1J,K). While GFP-β1A integrin formed long and thin central adhesions, resembling fibrillar adhesions, GFP–β1D integrin formed short peripheral and centrally located cell matrix adhesions (Fig. 1H-K). Quantification of adhesion length of C2C12 myoblasts plated on FN using a fully automated procedure (see Materials and Methods) revealed a threefold shorter average adhesion length with \$1D integrin compared to \$1A integrin (Fig. 1L), but with exaggerated adhesion length resulting from difficulties in separating individual adhesions. To confirm the adhesion length differences obtained by the automatic procedure, we also performed the adhesion length measurements by tracing the adhesions manually. We subsequently plotted the length distribution profile of all the traced adhesions for cells transfected with GFP–β1A integrin, GFP–β1D integrin as well as β3 integrin–GFP (Fig. 1M). This analysis revealed a mean adhesion length of 6 μm for the GFP-β1A integrin, while both the GFP-\(\beta\)1D integrin and \(\beta\)3 integrin-GFP formed shorter adhesions of 2–3 µm (Fig. 1N). This confirmed the notion that the composition of the β1 integrin cytoplasmic tail strongly affects the shape and potential function of cell matrix adhesions.

$\beta 1 \text{A}$ integrin induces fibronectin remodeling while $\beta 1 \text{D}$ integrin mediates adhesion

The increased adhesion length and central location of \$1A integrin adhesions suggested the formation of fibrillar adhesions, which have been shown to be involved in the remodeling of FN and deposition of new FN fibers (Pankov et al., 2000; Zamir et al., 2000). To confirm this notion, we performed co-staining of β1A integrin-transfected C2C12 myoblasts plated on laminin-111coated surfaces and evaluated the deposition of FN. Anti-FN staining revealed co-localization of GFP-\beta1A integrin with FN fibrils (Fig. 2A–D), suggesting FN-binding and the capacity to remodel extracellular FN by β1A integrin. In contrast, GFP-β1D integrin-transfected C2C12 cells recruited FN into short central adhesions, localizing to the ends of stress fibers. During cell displacement, these FN patches were deposited onto the laminin surface without forming a network of FN fibrils (Fig. 2E-H). This proposes that β1D integrins play a role in cell anchorage, but fail to remodel the extracellular matrix.

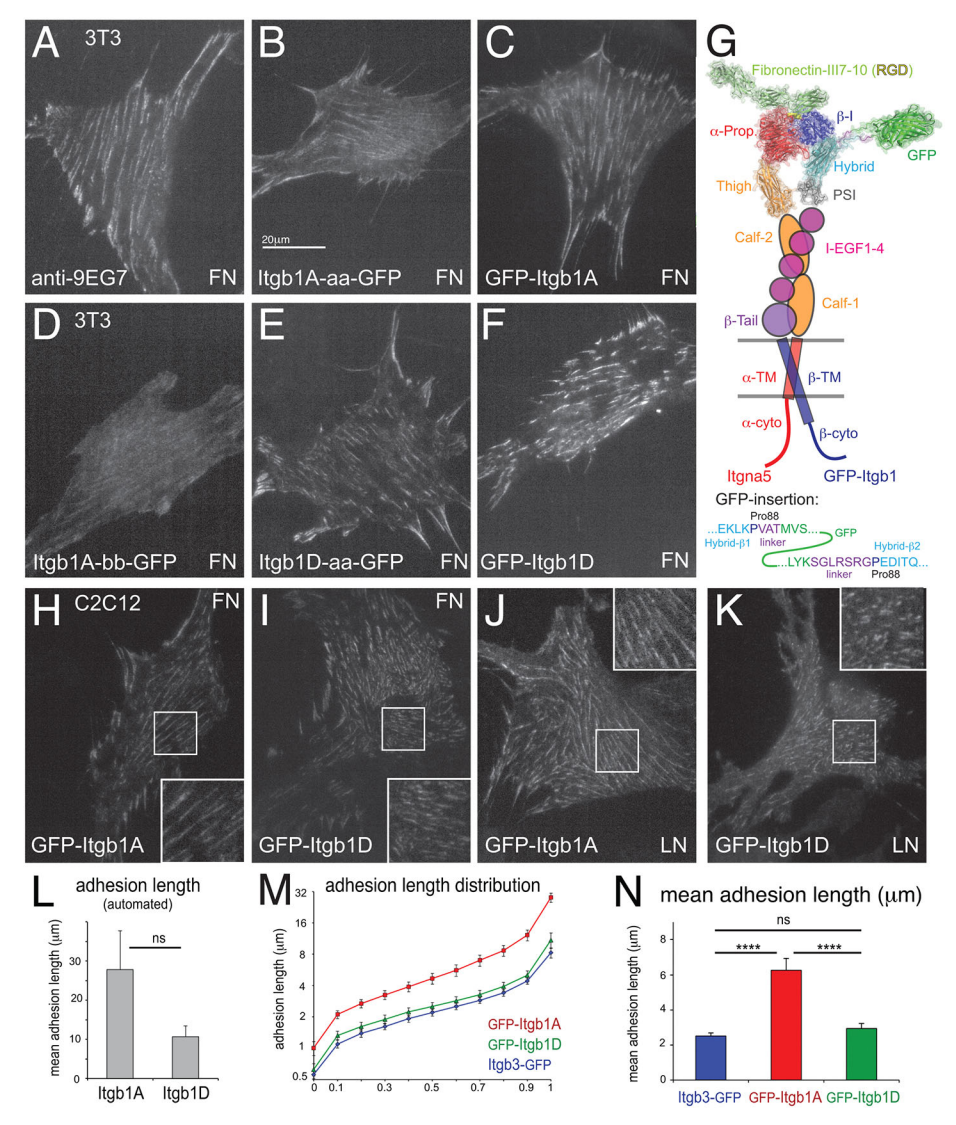


Fig. 1. Expression of GFP-tagged β1 integrin splice variants and adhesion length analysis. Representative TIRF images from three independent experiments, showing endogenous β1 integrin (A) or transiently transfected GFP-tagged β1 integrin splice variants in NIH 3T3 (A–F) and C2C12 cells (H–K) cultured for 8 h on FN- (A–F,H,I) and laminin (LN)-coated (J,K) glass coverslips. Endogenous, substrate-bound β1 integrin was labeled using clone 9EG7 (anti-CD29) antibody staining, showing centrally located fibrillar adhesions and peripheral focal adhesions (A). Cell expressing a C-terminally GFP-tagged β1A integrin, with a linker previously used for β3–GFP integrin (Ballestrem et al., 2001) (ltgb, β integrin) (B), or extracellularly GFP-tagged β1A integrin according to Egervari et al. (2016) (C,G). The integrin staining patterns were also compared to cells transfected with a C-terminally GFP-tagged β1A integrin with an 18-amino-acid, highly flexible linker (GGGGARRRGQAGQAGDPPVAT) (D), described in Parsons et al. (2008). Centrally located short adhesions were observed with both C-terminally (E), and extracellularly (F) tagged β1D integrin splice forms. (G) Structure based model of extracellularly GFP-tagged α5β1 integrin receptor with insertion site at P88, based on published structures α5β1 (3VI4), GFP (1C4F) and fibronectin type III repeats 7–10 (1FNF). An animated view of the integrin–GFP fusion model is shown in Movie 1. (H–K) Expression of extracellularly tagged β1A (H,J) and β1D integrin (I,K) splice variants in mouse C2C12 cells plated for 8 h on FN- (H,I) or LN- (J,K) coated coverslips. (L–N) Quantification of extracellular-tagged β1A and β1D integrin adhesion length distributions from TIRF images of transiently transfected C2C12 cells (n=3), plated for 8 h on FN-coated glass coverslips, using a non-supervised segmentation (L) (3×20 cells analyzed, mean±s.e.m., paired t-test), or a blinded, manual tracking approach (M,N) (adhesions from 3×8 cells analyzed, mean±s.e.m., one-way

In order to visualize such FN remodeling by $\beta1A$ integrin or cell anchorage by $\beta1D$ integrin, we performed time-lapse and FRAP analysis of cell-surface exposed GFP– $\beta1A$ integrin and GFP– $\beta1D$ integrin in transiently transfected C2C12 cells plated on FN-coated surfaces. GFP– $\beta1A$ integrin was found in elongated fluorescent structures or patches localized underneath the main cell body. These structures probably represented fibrillar adhesions, as such structures were associated, but not co-localized with focal adhesions, identified as dark zones by interference reflection microscopy (Fig. 3A, asterisks). Consistent with FN polymerization

in fibrillar adhesions, GFP– $\beta1A$ integrin patches moved and appeared to be elongated into linear structures, giving the impression that the cell translocated FN-bound $\alpha5\beta1A$ integrins on the cell surface (Fig. 3A, arrows, insert). We also analyzed integrin dynamics within such fibrillar adhesions with fluorescence recovery after photobleaching (FRAP) and noted a recovery of the fibrillar integrin fluorescence (Fig. 3B, arrow), suggesting a dynamic linkage of GFP– $\beta1A$ integrin to FN fibrils (Fig. 3B,E). In contrast, analysis of GFP– $\beta1D$ integrin-containing cell matrix adhesions revealed adhesion structures that were either directly

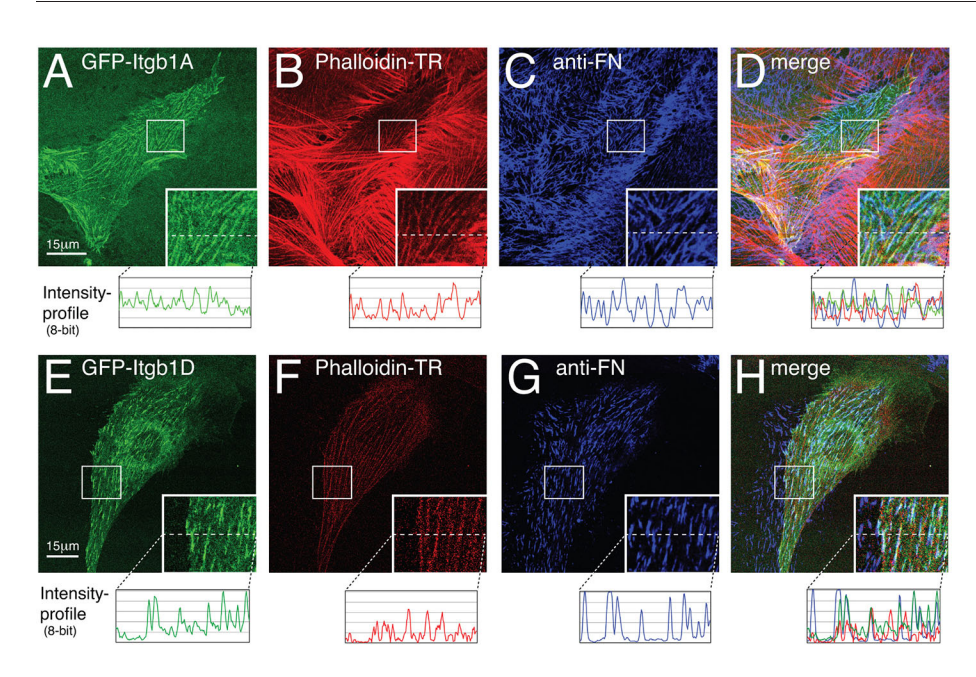


Fig. 2. FN assembly of extracellularly GFP-tagged β 1A and β 1D integrins in C2C12 cells. Representative confocal images (A–H) of transiently transfected GFP– β 1A integrin or GFP– β 1D integrin in C2C12 cells plated overnight on laminin-coated glass coverslips (A–H) and imaged for β 1A integrin (GFP; A), β 1D integrin (GFP; E), F-actin [phalloidin–Texas Red (TR); B, F] or deposited fibronectin (anti-FN; C,G), and their merge (D,H). Intensity profiles were drawn through the magnified area (dotted lines) to reveal co-localization of F-actin, FN and β 1 integrin.

bound to the FN-coated glass coverslip (interference reflection dark contacts) (Fig. 3C, asterisks) or organized in a patchy or elongated manner underneath the main cell body, suggesting association with short FN fibrils (Fig. 3D; Movie 2). In both cases, FRAP analysis revealed almost no fluorescence recovery over a period of 20 min, suggesting that the adhesive interaction of GFP– $\beta1D$ integrin with the extracellular ligand was stable and the attachment sites were not remodeled (Fig. 3C–E). These data reveal a dynamic interaction of $\beta1A$ integrin with the cytoskeleton and are in agreement with its role in the remodeling of the extracellular matrix (Pankov et al., 2000). In contrast, $\beta1D$ integrin fails to show such dynamic remodeling, creating highly stable and matrix-immobilized adhesion sites, which may reflect its role as a muscle-specific integrin.

To confirm that both $\beta1A$ and $\beta1D$ integrins were properly anchored to the actin cytoskeleton, we stained cells transiently transfected with these constructs with anti-vinculin (Fig. 3F–I), revealing co-localization for both of them (Fig. 3F,G). In contrast, C-terminally GFP-tagged $\beta1A$ integrin, which was present in the cell membrane, failed to be recruited into vinculin-positive adhesions (Fig. 3I). This suggests a critical role of the C-terminal tail for $\beta1A$ integrin recruitment to cell matrix adhesions, which was less important for $\beta1D$ and $\beta3$ integrins (Fig. 3H).

C-terminal truncation revealed isoform-specific requirement of the distal NPXY motif

The robust recruitment of extracellularly tagged $\beta1A$ integrin into focal and fibrillar adhesions, which was not seen with C-terminally tagged $\beta1A$ integrin, suggested that the distal NPXY-motif or part of the C-terminal integrin sequence was critical for the recruitment of $\beta1$ integrins into cell matrix adhesion sites. To test this hypothesis, we analyzed extracellularly tagged, C-terminally truncated $\beta1A$ and $\beta1D$ integrins for their ability to localize into cell matrix adhesions (Fig. 4A–C). The deletion of the C-terminal Lys (K798) residue did not affect $\beta1A$ integrin recruitment into cell matrix adhesions (Fig. 4B). In contrast, deletion of the three or four C-terminal residues, which in the latter case included the deletion of Y795, resulted in progressive loss of the ability of the GFP– $\beta1A$ integrin variants to be recruited into cell matrix adhesions (Fig. 4B). However, when performing a similar C-terminal deletion for $\beta1D$ integrin, for example removing the last seven C-terminal residues

including Y795 (β 1D delY795), the resulting mutant was still recruited to cell matrix adhesions with a similar pattern to that observed for the full-length GFP- β 1D integrin (Fig. 4C). This revealed independence of the distal NPXY motif from β 1D integrin recruitment and explained focal adhesion recruitment of C-terminally tagged β 1D integrin (Fig. 1). The C-terminus of β 1A integrin displayed a tolerance for deletion of the last amino acid, but a requirement for Y795 and a free C-terminus for full activity was observed as previously suggested (Fitzpatrick et al., 2014).

Previous work has proposed a critical role for integrin adapter proteins such as kindlins and sorting nexins for the efficient cell-surface expression of integrins (Margadant et al., 2012; Tseng et al., 2014). Since these adapters bind to the C-terminal parts of integrin β tails, a lack of recruitment of truncated β 1A integrin into adhesions could be easily explained by a failure of integrin maturation or cell-surface expression. However, because of low transfection efficiency of our constructs in 3T3 and C2C12 cells, we did not conduct further biochemical and cell biological tests at this point, but instead confirmed the relevance of these C-terminal sequences for β 1A integrin for recruitment into focal or fibrillar adhesions.

Proline 786 is critical for creating stable $\beta 1D$ integrin adhesions

A previous structural analysis of the β1D integrin–talin2 complex proposed an interaction of P786, as well as some minor interactions of N788 and N789 with the talin2 F3 domain (Anthis et al., 2010, 2009). In addition, these authors measured a two- to threefold reduction in β1D-talin2 affinity as a result of P786A and Q778G mutations (Anthis et al., 2010). To test if these residues, or possibly the 3-amino acid extension in β1D, were involved in the differential integrin clustering phenotype observed between the β1A and β1D integrins, we created GFP-β1D Q778G, GFP-β1A G778Q, GFP-β1A addAGL, GFP-β1D P786A, and GFP-β1D N788T/ N789T mutant integrin constructs and expressed them in 3T3 cells (Fig. 4D). The GFP-β1D Q778G and GFP-β1A G778Q mutations (data not shown), as well as GFP-β1A addAGL (Fig. 4D), showed very similar adhesion patterns in comparison to their control constructs and we did not further pursue their analysis. In addition, the GFP-β1D N788T/N789T mutant integrin showed extensive

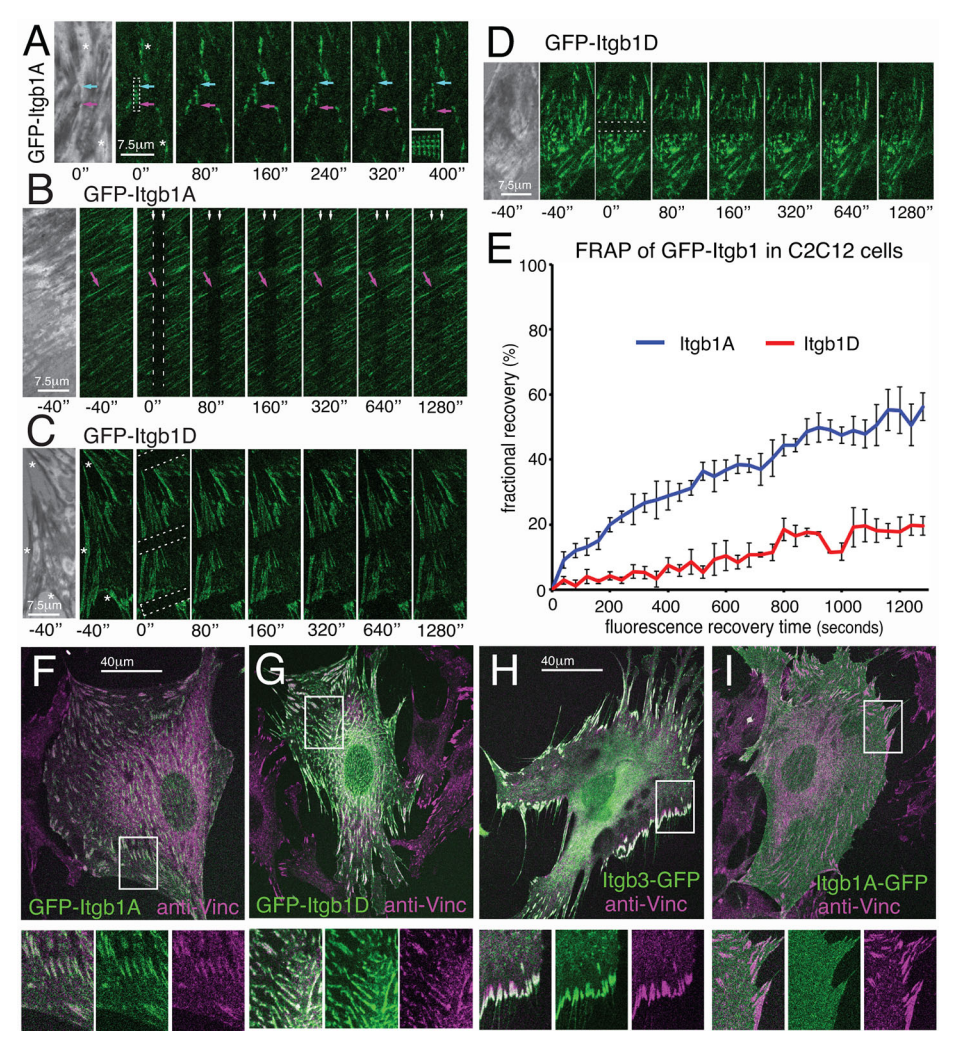


Fig. 3. FN assembly, turnover dynamics and vinculin adapter recruitment of extracellularly GFP-tagged β1A and β1D integrins in C2C12 cells. (A–D,F–I) Representative confocal images of time-lapse or FRAP analysis of transiently transfected C2C12 cells plated on FN-coated glass coverslips. (A) Time-lapse analysis of C2C12 cells transfected with GFP-β1A integrin and cultured for 72 h revealed dynamic changes in integrin distribution, illustrated by an elongating patch of GFP-β1A integrin fluorescence (between arrows, and boxed region shown as a kymograph in the last frame). Please note the localization of integrin-positive patches (asterisks) close to interference reflection-dark zones of cell–substrate adhesions. (B–E) FRAP analysis (bleached regions indicated by dashed lines) of C2C12 cells transfected with either GFP-β1A integrin (B) or GFP-β1D integrin (C,D) and plated on FN-coated coverslip for 30 h (B), 5 h (C) and 72 h (D) (Movie 2). An interference reflection image is shown at the beginning of each sequence showing whether the GFP-labeled structures are directly bound to glass-coated FN (interference reflection-dark areas) (C, asterisks), or partially-detached FN-fibrils (B,D). (E) Quantification of the fluorescence recovery of bleached adhesion structures (as indicated by an arrow in B). Data points represent the mean±s.e.m. of 3–4 cells per condition, each with 3–5 analyzed adhesions. With the exception of the first data point at 40 s, a paired *t*-test showed significant differences (*P*<0.05) for all later time points. (F–I) Anti-vinculin antibody stained (anti-Vinc, magenta) C2C12 cells transfected with different integrins and plated overnight on FN-coated coverslips revealing extracellularly tagged GFP-β1A integrin (F), GFP-β1D integrin (G), β3–GFP integrin (Ballestrem et al., 2001) (H), and C-terminally GFP-tagged β1A integrin-aa–GFP as in Fig. 1B (I). Note the membrane staining of the C-terminally tagged β1A integrin-aa–GFP, and apparent absence from vinculin-positive central adhesions (compare F

central adhesion formation, resembling the original GFP $-\beta1D$ integrin-transfected cells (Fig. 4D). However, the P786A mutation in GFP $-\beta1D$ integrin caused the loss of all centrally located adhesion sites, an increase in cell membrane-localized staining and an enlargement of peripheral focal adhesions (Fig. 4D). In addition, focal adhesions had a tendency to slide and cell edges retracted easily in the $\beta1D$ P786A integrin mutant (Movie 5). Interestingly, localization into peripheral inward sliding adhesions resembled the phenotype observed in $\beta3$ integrin—GFP transfected 3T3 cells (Ballestrem et al., 2001; Cluzel et al., 2005) (Fig. 5C,D). Since the P786A mutation changed the behavior of GFP $-\beta1D$ integrin, we wondered whether the reciprocal A786P conversion in GFP $-\beta1A$ integrin had a similar strong effect. Cells transiently transfected with

this reciprocal mutation exhibited long thin central adhesions, reminiscent of fibrillar adhesions, but the cells appeared less anchored in their peripheries (Fig. 4D).

To further evaluate the similarities between the dynamics of β3 integrin–GFP and GFP–β1D P786A, FRAP analysis of transiently transfected 3T3 cells was performed. Similarly to β3 integrin–GFP-transfected 3T3 cells, this analysis revealed a complete fluorescence recovery of focal adhesion fluorescence within 10–15 min for GFP–β1D P786A (Fig. 5C,E), GFP–β1A integrin (Fig. 5A,E) and β3 integrin–GFP (Fig. 5D,E), contrasting with the immobile phenotype of the β1D integrin isoform (Fig. 5B,E).

To verify that the differential dynamics of GFP $-\beta1A$ and GFP $-\beta1D$ integrin were not due to endogenously expressed $\beta1A$ integrin, we

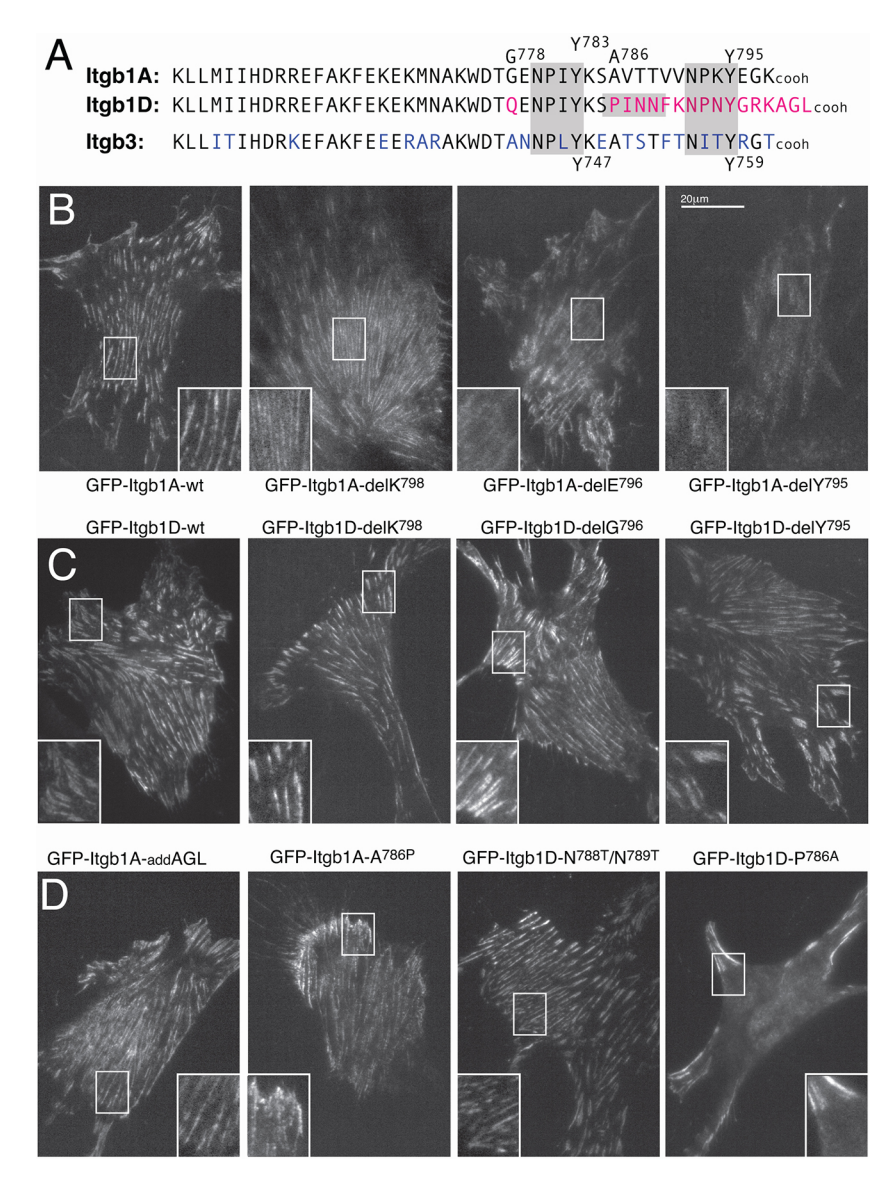


Fig. 4. Mutational analysis of GFP-β1A integrin and GFP-β1D integrin adhesion formation in NIH 3T3 cells. (A) Sequence comparison between the cytoplasmic tails of \$1A, \$1D and \$3 integrins and indication of the conserved proximal and distal NXXY motifs (gray boxes) as well as the sequence differences in the inter-NPXY region, PINNFK in integrin β1D. Residues differing from β1A integrin are highlighted in red and blue for β1D and β3 integrins, respectively. (B-D) Representative TIRF images of NIH 3T3 cells plated for 8 h on FN-coated glass coverslips, transiently transfected with wild-type or mutant versions of extracellularly GFP-tagged $\beta1A$ or $\beta1D$ integrins as indicated. (B,C) Representative images of C-terminal deletion series of $\beta1A$ (B) or $\beta1D$ integrins (C). Note the progressive loss of adhesion formation in C-terminally truncated β1A but not β1D integrin. (D) Sequence swapping between $\beta1A$ and $\beta1D$ integrins, revealing a partial loss-offunction phenotype in the β1D P786A integrin mutant.

stably expressed these GFP– $\beta1$ integrins in $\beta1$ integrin-deficient GD25 cells. Similarly to the behavior in C2C12 and 3T3 cells, the fast and slow dynamic exchange of GFP– $\beta1A$ and GFP– $\beta1D$ integrin, respectively, was also found in GD25 cells (Fig. 5F), suggesting that integrin dynamics is controlled by its C-terminal tail sequence. The difference in adhesion dynamics in these transfected GD25 cells was also illustrated by measuring the displacement of the edges of cell matrix adhesion, analyzed from time-lapse recordings across 5 h. The mean adhesion speeds of all measured adhesions was about 1.5× faster for GFP– $\beta1A$ integrin adhesions compared to GFP– $\beta1D$ integrin adhesions [n=6 cells; >2000 measurements per cell, 18.0± 5.1 μ m/h (mean±s.e.m.) for GFP– $\beta1A$ integrin, and 11.5±0.9 μ m/h for GFP– $\beta1D$ integrin]. This trend was even more pronounced for the fraction of the 50% fastest moving adhesions (25.3±7.8 μ m/h for GFP– $\beta1A$ integrin, and 14.8±1.2 μ m/h for GFP– $\beta1D$ integrin).

Reduction of cell attachment forces by the $\beta 1D$ P786A mutation

In order to analyze whether the enhanced integrin dynamics of the β 1D P786A integrin mutant would affect β 1 integrin-dependent cell-matrix attachment forces, we tested the resistance to fluid shear forces by employing a spinning disc assay (Friedland et al., 2009;

Tabone-Eglinger et al., 2014). Transiently transfected β1 integrindeficient GE-11 cells were plated on FN-coated coverslips and exposed to fluid shear stress in a spinning disk device. A soluble DsRed construct was co-expressed with extracellularly tagged GFP–β1A or GFP–β1D integrin in GE-11 cells for 72 h. Transiently transfected cells were then detached and plated onto circular coverslips for 30 and 60 min, prior to subjection to shear forces in the spinning disc device for 5 min. In order to prevent β3 integrindependent cell attachment to FN, we incubated cells in the presence of the $\alpha v \beta 3$ - and $\alpha v \beta 5$ -specific inhibitor S-36578-2 (Maubant et al., 2006), efficiently reducing FN-mediated cell attachment forces of non-transfected GE-11 cells at concentrations of 400 nM (data not shown). Under these conditions, which blocked the adhesive response by endogenous β3 integrin, attachment forces for GE-11 cells transfected with GFP-\beta1A or GFP-\beta1D integrin were remarkably similar. By contrast, the expression of the GFP–β1D P786A integrin receptor in GE11 cells led to a twofold reduction in shear resistance (Fig. 5G). Thus, despite the reported differences in talin-binding affinities between \$1A and \$1D integrin, and the different integrin turnover rates in adhesions, the two \$1 integrin splice variants induced the same cellular resistance to mechanical shear forces. Nevertheless, a reduction in shear resistance was seen

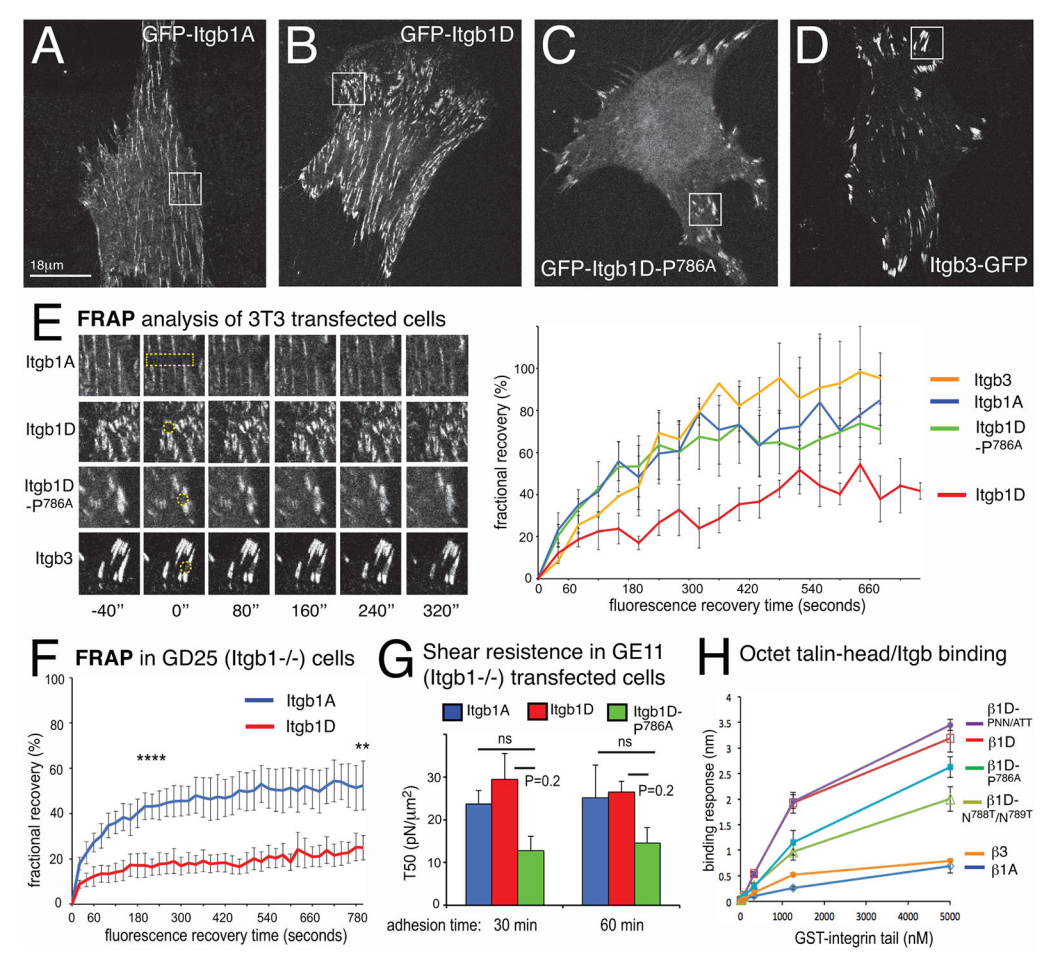


Fig. 5. FRAP and cytoplasmic adapter recruitment analysis in wild-type and P786A mutant β 1D integrins. (A–E) Confocal imaging and FRAP analysis of extracellularly tagged wild-type GFP– β 1A integrin (A) (Movie 3), GFP– β 1D integrin (B) (Movie 4), GFP– β 1D P786A integrin (C) (Movie 5) and C-terminally tagged β 3–GFP integrin (D) (Movie 6) (Ballestrem et al., 2001), transiently transfected into NIH 3T3 cells and plated onto FN-coated glass coverslips prior to FRAP analysis (E). Area outlined with yellow dotted line indicates bleached areas. FRAP curves were established from at least three independent cells with three different adhesions per cell (mean±s.e.m.). (F) In order to exclude an influence of expression levels, or of endogenous β 1A integrins, the FRAP analysis was repeated in stably transfected β 1 integrin-deficient (ltgb-/-) GD25 cells expressing extracellularly GFP-tagged β 1A (Movie 7) and β 1D (Movie 8) integrins (n=5 cells with 3–5 analyzed adhesions; mean±s.e.m., paired t-test), showing significantly different fluorescence recovery during the recovery phase (****P<0.0001) or at the end of the analysis period for the mobile fractions (**P<0.01). (G) Spinning disk analysis of the shear force resistance of β 1 integrin-deficient (ltgb-/-) GE11 cells on FN-coated coverslips, transiently transfected with different β 1 integrins and inhibited with an α v β 3 intergrin inhibitor. Note the lack of significant differences in shear force resistance between GFP- β 1D integrin and GFP- β 1D integrin, and more substantial, but still non-significant, reduction for the GFP- β 1D P786A integrin mutant (mean±s.e.m., one-way ANOVA; ns, not significant) (H) Biolayer interference analysis (Octet biosensor) of GST- β integrin tail fusion protein binding to His-tagged talin1 FERM domain (residues 1–405) (n=3, mean±s.e.m.). Note the twofold reduction in talin1 affinity for the β 1D P786A integrin mutant, but fivefold lower affinities of β 1A and β 3 integrin tails as compared to integrin β 1D.

in the $\beta1D$ P786A mutant integrin isoform. These findings suggest that mechanical adhesion to matrix is an integrated response in which reduced adapter binding affinities can be compensated by changes in avidity or integrin clustering, and may also include integrin-dependent signaling to maintain the focal adhesion, in order to resist an increase in shear forces.

Lack of correlation between talin-integrin affinity and cell-matrix adhesion behavior

In order to understand whether talin–integrin affinity differences were responsible for the above-mentioned changes in cell matrix adhesion phenotypes, we decided to directly measure the binding affinity of GST-fused $\beta 1$ integrin tails to immobilized talin1 head domain (amino acids 1–405). The talin1 head was immobilized on a sensor surface and the binding of GST- $\beta 1A$ integrin tail fusion proteins was analyzed by biolayer interferometry as previously described for $\beta 3$ integrin tails (Pinon et al., 2014). We observed

enhanced binding of $\beta1D$ over $\beta1A$ and $\beta3$ integrin tails to the immobilized talin head domain (Fig. 5H). The $\beta1D$ P786A and the $\beta1D$ N788T/N789T mutant integrin tails showed about half the talin-binding capacity of $\beta1D$ integrin, but still twice as much as the $\beta1A$ and $\beta3$ integrin tails. Interestingly, the binding affinity for the triple mutant ($\beta1D$ P786A/N788T/N789T) was again identical to $\beta1D$ integrin, demonstrating that talin–integrin affinity is not easy to predict based on individual mutations (Fig. 5H).

Talin2 induces recruitment of β 1D integrins to central adhesions

In order to further evaluate the recruitment mechanisms of $\beta1D$ or $\beta1A$ integrins into central and peripheral adhesions, we tested the localization of the two talin isoforms in C2C12 cells. As previously reported (Austen et al., 2015; Rahikainen et al., 2017), expression of talin1–mCherry was mainly restricted to peripheral adhesions (Fig. 6A), where $\beta3$ and $\beta1A$ integrin can be detected in fibroblast

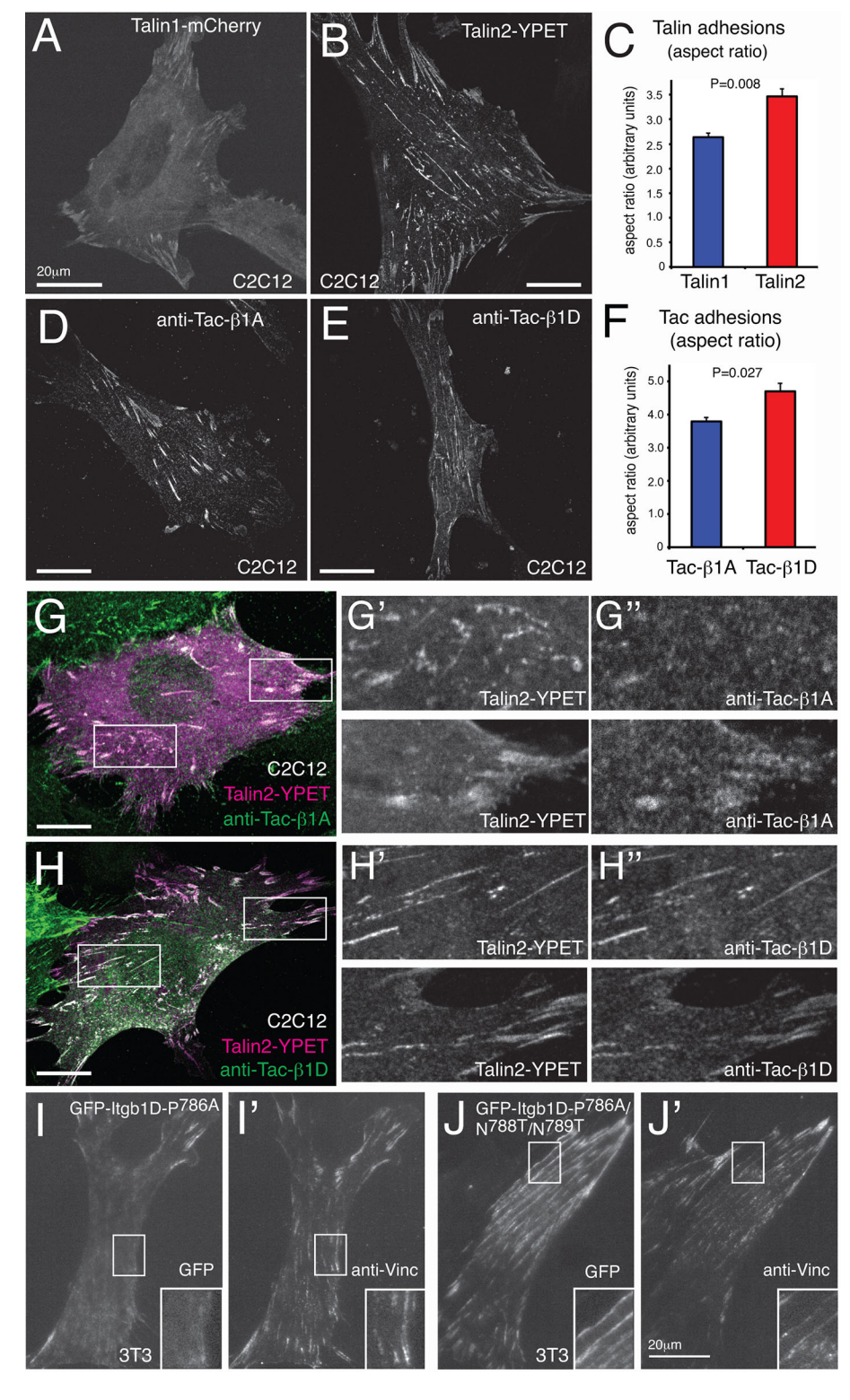


Fig. 6. Analysis of central adhesions for talin2 and \$1D integrin recruitment. Representative confocal and TIRF images from three independent experiments showing transiently or stably transfected C2C12 (A,B,D,E,G-H"), or NIH 3T3 cells (I-J'), expressing C-terminally tagged talin1 or talin2, as well as the Tac-β1A integrin or Tac–β1D integrin chimera. (A,B) Transient transfections of C2C12 cells with talin1-mCherry (A) and talin2-YPet (B), and the evaluation of the aspect ratios of talin-positive adhesions (*n*=3) with eight cells per condition (mean±s.e.m., paired t-test) (C). (D,E) Anti-Tac antibody (clone 7G7) staining of stably transfected and bulk sorted C2C12 cells expressing Tac–β1A integrin (C) and Tac-β1D integrin (D). Cells were plated on serum-coated glass coverslips for 24 h prior to fixation and imaging. Subsequent aspect ratios of Tac-positive adhesion structures were determined from three different batches of plated cells (n=3, with eight cells per condition, mean±s.e.m., paired t-test) (F). (G-H") Transient transfection of talin2-YPet into stably transfected C2C12 cells expressing Tac-β1A integrin (G) or Tac-β1D integrin (H). Representative cells were selected from three independent experiments and co-localization was determined by confocal microscopy and comparison of the individual signals of talin2-YPet (G',H') and anti-Tac antibody (G",H"). Please note the extensive overlap of central (upper panels) and peripheral adhesions (lower panels) between the talin2 and Tac–β1D integrin construct (H), and reduced overlap of talin2 and Tac-β1A integrin construct in central adhesions (G',G", upper panels). (I-J') TIRF imaging of anti-vinculin antibody labeled NIH 3T3 cells transiently transfected with extracellular GFP-tagged β 1D P786A (I) and β 1D P786A/N788T/N789T (J) mutant integrins. Note the absence of recruitment to central adhesions in the B1D P786A integrin mutant, and recovery of fibrillar adhesion-like central adhesions in the triple β1D P786A/N788T/N789T mutant, respectively.

cells. Interestingly, the expression of a talin2–YPet construct (Austen et al., 2015) revealed centrally located fibrillar adhesions, as well as staining in peripheral focal adhesions (Fig. 6B), similar to the data reported by Praekelt et al. (2012). Quantification of the adhesion length and diameter showed significant differences in the aspect ratio (major axis:minor axis) of the talin1 and talin2 adhesions (Fig. 6C). With the help of previously described fusion proteins of the extracellular domain of the IL2 receptor alpha (Tac, also called IL2RA) (LaFlamme et al., 1994) and the transmembrane and

cytoplasmic domain of either $\beta1A$ or $\beta1D$ integrins (Tac- $\beta1A$ integrin and Tac- $\beta1D$ integrin), we probed the intracellular recruitment of these constructs to the membrane-proximal cytoskeleton of C2C12 cells. While Tac- $\beta1A$ integrin was recruited to peripheral and centrally located large and wide focal adhesions (Fig. 6D), Tac- $\beta1D$ integrin localized to thin elongated fibrillar adhesion-like structures (Fig. 6E), very similar to the adhesions labeled with talin2. We confirmed this differential pattern by establishing the aspect ratio of the measured Tac

localization, which revealed similar patterns for talin2 and Tac- $\beta1D$ integrin (Fig. 6F). Furthermore, talin2 transfection into C2C12 cells stably transfected with Tac- $\beta1A$ integrin or Tac- $\beta1D$ integrin revealed extensive co-localization in both central and peripheral adhesions for talin2 and Tac- $\beta1D$ integrin, but only an overlap in staining of peripheral adhesions for talin2 and Tac- $\beta1A$ integrin (Fig. 6G,H). Thus, using Tac-integrin chimeras as affinity probes, our data suggested that $\beta1D$ integrin is recruited to central and peripheral adhesions in a talin2-dependent manner, while $\beta1A$ integrin shows a preferred interaction with talin1, localized in peripheral focal adhesions.

As shown above, when bound to their extracellular ligands, β1D integrin forms short and substrate-anchored adhesions in the cell center, while \(\beta \) IA integrin forms centrally located, long and thin FN-associated fibrillar adhesions (see Fig. 2). This suggests that retention of \$1A integrin in fibrillar adhesions requires talin2 and additional cytoskeletal elements. By contrast, mutations targeting the residue P786 in \(\beta 1D \) integrin (Fig. 4D) may cause the loss of recruitment to such talin2-enriched central adhesions. Therefore, we further evaluated the connection of the GFP-β1D P786A integrin mutant with other elements of the cytoskeleton. Transiently transfected 3T3 cells were stained for endogenous vinculin in order to potentially identify changes in adapter interactions. Indeed, the P786A mutation led to the loss of GFP-β1D integrin co-localization with vinculin-expressing central fibrillar adhesions (Fig. 6I), suggesting that a specific centrally located F-actin interaction capacity has been lost as a result of the P786A mutation in GFP-β1D integrin. However, when the P786A loss-of-function mutation was combined with the N788T/N789T mutation (GFP–β1D P786A/N788T/N789T), long and thin centrally located cell matrix adhesions were again detected (Fig. 6J), resembling the phenotype of GFP-β1A integrin. In addition, these central adhesions were also positive for anti-vinculin staining (Fig. 6J), proposing that a loss in β1D integrin affinity for talin2 resulting from the P786A mutation, could be at the origin of the β3 integrin-GFP-like adhesion behavior. In contrast, the capacity of GFP-\beta1A integrin to assemble FN fibers might be critically linked to residues T788 and T789 that are expressed in \(\beta 1 \) integrin in the context of alanine at position 786. Interestingly, the same two threonine residues, T788 and T789, have previously been identified to be required for binding to integrin adapter kindlin proteins (Moser et al., 2008), suggesting that kindlin recruitment to the integrin tail also determines the differential organization and dynamics of focal and fibrillar adhesions.

P786 prevents paxillin recruitment and cell spreading in $\beta 1D$ integrin

Since integrin adhesion dynamics are also regulated by cellular signaling activity (Tabone-Eglinger et al., 2012) and not only by integrin—adapter protein affinity, we analyzed the signaling capacity of cell matrix adhesion sites by staining with anti-paxillin and anti-phospho-tyrosine antibodies, qualitatively showing the same result. In contrast to anti-vinculin, anti-phospho-tyrosine staining did not reveal centrally located fibrillar adhesions in GD25 cells stably transfected with GFP– β 1A integrin, but stained mainly the peripheral focal adhesions (Fig. 7A). In contrast to anti-vinculin staining in GFP– β 1D integrin-expressing 3T3 cells, phosphotyrosine proteins were not efficiently recruited to GFP– β 1D integrin-containing adhesions in GD25 cells (Fig. 7B). Interestingly, expressing β 1D integrins in GD25 cells also had a negative effect on their spreading capacity. Moreover, after 6 h of

spreading on FN, a reduction in the cell area was observed for $GFP-\beta 1D$ integrin-expressing cells (Fig. 7I).

One of the central signaling adapter proteins in focal adhesions is paxillin, whose recruitment to β3 integrin-containing adhesions correlates with cell spreading (Pinon et al., 2014). While antipaxillin staining was detected in peripheral GFP-β1A integrincontaining focal adhesions (Fig. 7C), anti-paxillin staining was barely detected in adhesion sites containing GFP–β1D integrin, GFP-β1A A786P or GFP-β1D P786A integrin (Fig. 7D-F). Interestingly, the GFP-\beta1A integrin with a proline mutation at position A786 (A786P) was still able to form centrally located fibrillar adhesions (Fig. 7D). When the localization of paxillin to GFP–β1 integrin-containing adhesion sites was evaluated by the Pearson coefficient (Fig. 7J), a significant reduction in paxillin recruitment was observed for both the GFP-β1D A786P and the GFP-B1A A786P mutant integrins as compared to GFP-B1A integrin. Additionally, and in order to exclude the 'contamination' of GFP-β1 integrins with endogenous β3 integrin, and thus with β3 integrin-dependent recruitment of paxillin, we used FN/ vitronectin (VN)-patterned substrates (Pinon et al., 2014), to spatially dissociate the \(\beta 1A\) and \(\beta 1D\) integrins from endogenous β3 integrins (Fig. 7G,H). Quantification of GFP-tagged integrin expression with respect to paxillin staining revealed a reduction of paxillin recruitment onto GFP–β1D integrin-containing adhesions on FN (Fig. 7K), confirming the results obtained by the evaluation of the localization correlation analysis on non-patterned surfaces (Fig. 7J). Thus, in addition to the observed increase in talinbinding affinity of the β1D integrin tail in vitro and slowed down integrin turnover (Fig. 3E; Fig. 5E,F), β1D integrin also caused reduced paxillin recruitment to adhesion sites and decreased cell spreading.

Paxillin recruitment to $\beta 1$ integrin correlates with cell proliferation

The reduced recruitment of paxillin to β1D integrin in GD25 cells was further analyzed to understand its potential impact on other integrin-dependent signaling events, such as cell proliferation. In order to reveal β1 integrin-dependent proliferation activity in SV40transformed GD25 cells, we used the xCELLigence system and analyzed cell proliferation by measuring the increase in electric impedance over 75 h as an indication of increasing substrate coverage and therefore cell number. GD25 cells stably transfected with GFP–β1A integrin or with GFP–β1D integrin (Fig. 7M) showed no dramatic changes in impedance during the first 20 h (Fig. 7N). Afterwards, GFP–β1A integrin-expressing cells started proliferating more quickly than GFP–β1D integrin-expressing cells, leading to a continuous delay in proliferation of the latter cell line of 7 h (Fig. 7N,O). Additionally, we tested cell proliferation in this setting by BRDU incorporation. We reduced the serum-mediated stimulation of proliferation by starving the cells for 20 h in 1% serum-containing medium, prior to the BRDU incubation for 4 h (Fig. 7L). Again, GD25 cells stably transfected with GFP-β1A integrin showed enhanced proliferation as indicated by increased BRDU incorporation compared to non-transfected control cells, or cells that expressed GFP-\beta1D integrin. Moreover, the expression of GFP–β1A integrin carrying the A786P mutation suppressed BRDU incorporation, even below that seen with non-transfected control cells. This suggests that P786 has an important role in B1D integrin to mechanically stabilize the talin-β1D integrin interaction, while also preventing recruitment of the paxillin signaling adapter protein to prevent adhesion signaling and adhesion turnover of β1D integrins in differentiated myotubes.

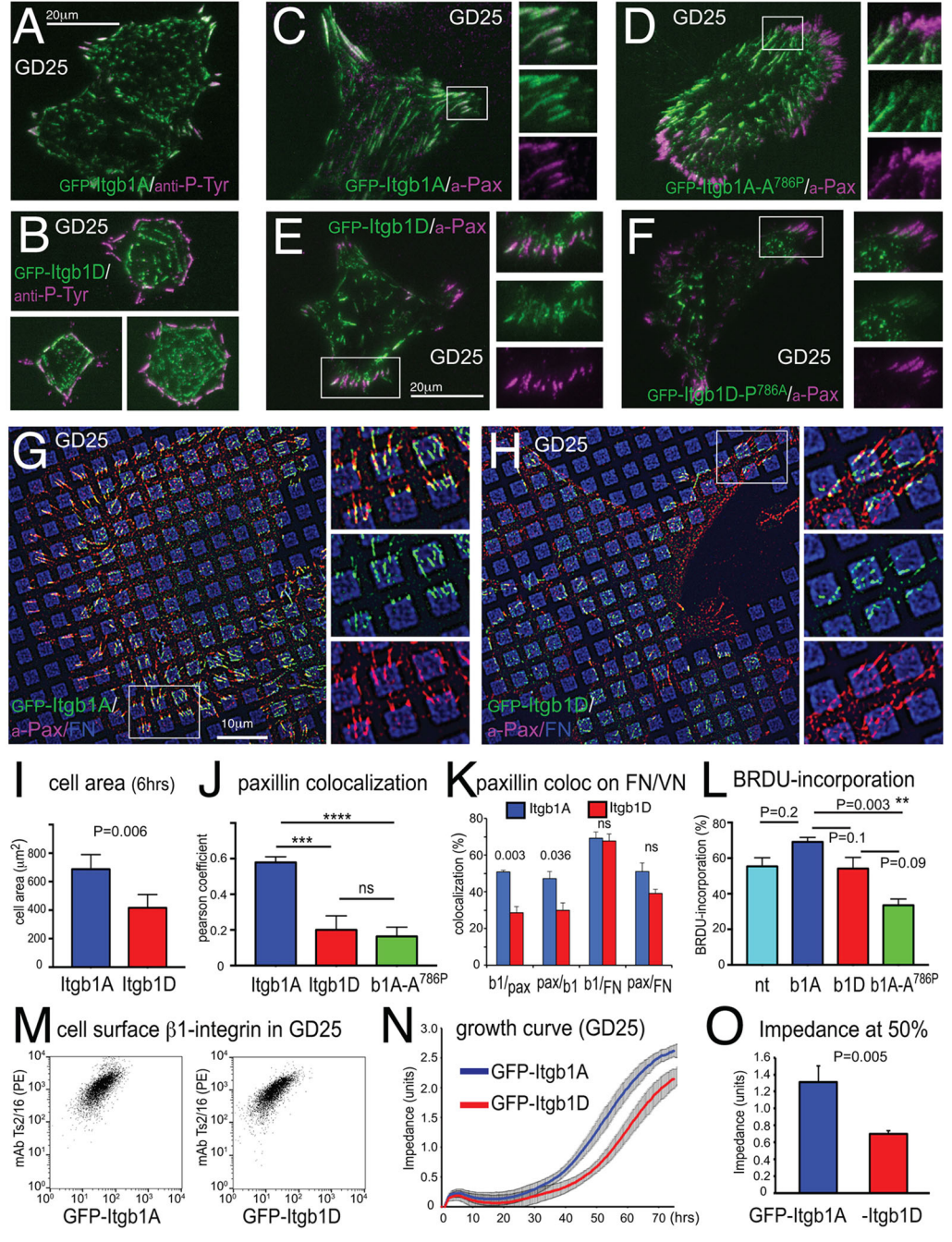


Fig. 7. Reduction in cell spreading and proliferation of β1D integrin-expressing cells correlates with reduced paxillin recruitment. (A–F) Representative images from three independent experiments showing TIRF imaging of stably transfected GD25 cells (A-F), plated for 6 h (A,B) or overnight (C-F) on FN-coated glass coverslips and stained with anti-phospho-tyrosine (anti-P-Tyr) (A,B) and anti-paxillin (a-Pax) antibodies (C-F). Note the absence of p-Tyr and paxillin staining in central fibrillar adhesions in wild-type β1A integrin-transfected cells (A,C), but also lack of co-localization in peripheral adhesions in cells transfected with GFP-tagged β 1A A786P integrin (D), β 1D integrin (E), and β 1D P786A integrin (F), (G.H) SIM microscopy of GD25 cells stably expressing GFP- β 1A integrin or GFP-\(\beta\)1D integrin plated on binary choice VN/FN-patterned substrates obtained by microcontact printing. (I) Quantification of the cell spreading area of GD25 cells stably transfected with GFP-β1A integrin or GFP-β1D integrin on FN-coated coverslips, 6 h after plating (15 cells per condition, n=3; mean±s.e.m., paired t-test). (J) Quantification of the Pearson coefficient from TIRF images comparing anti-paxillin staining and GFP-β1 integrin fluorescence from cells plated overnight on FN-coated coverslips (10 cells analyzed per condition, n=3; mean±s.e.m., one-way ANOVA; ***P<0.001; ****P<0.0001; ns, not significant). (K) Quantification of co-localization of GFP-β1A integrin or GFP-β1D integrin with paxillin and FN on VN/FN binary choice patterns (10 cells for each condition, n=3, mean±s.e.m., paired t-test). (L) BRDU incorporation assay into GD25 cells stably expressing GFP–β1A integrin, GFP–β1D integrin or GFP–β1A A786P mutant integrin (n=3, >250 cells per condition, mean±s.e.m., one-way ANOVA, **P<0.01). Note the significant reduction in BRDU incorporation of the A786P mutant compared to wild-type β1A integrin. Although similar to non-transfected cells, the reduction of BRDU incorporation of β1D integrin was not significantly different from wild-type β1A integrin-transfected cells. (M) Representative FACS and dot-blot analysis of stably transfected GD25 cells exhibiting GFP-β1A integrin or GFP-β1D integrin on their surfaces. The intensity of GFP fluorescence (x-axis) is plotted against surface staining with clone Ts2/16 (anti-CD29) antibody, which does not stain non-transfected GD25 cells. (N,O) 75 h growth curve of stably transfected GD25 cells (n=3, mean±s.e.m., t-test), revealed by impedance measurement in an xCELLigence system. The histogram in O shows the impedance measurement of both cell lines at the time the half-maximal level of impedance was reached by the GFP-β1A integrin transfected cells (n=3, mean±s.e.m., paired t-test).

DISCUSSION

The development and regeneration of muscle tissue is intimately linked to changes in the expression of the integrin family of receptors and their association with different ECM structures. During development, myoblasts of somitic origin (Chevallier, 1979) invade the limb mesenchyme along migration pathways that provide an ectoderm- or fibroblast-secreted FN-containing matrix (Chiquet et al., 1981; de Almeida et al., 2016). While individual myoblasts can also secrete and organize their own FN network, the FN network is lost from the surfaces of fused myotubes (Chen, 1977; Chiquet et al., 1981). Moreover, the interaction with FN stimulates the proliferation of myoblasts, while also delaying their fusion into myotubes (Podleski et al., 1979). In addition, the regeneration of myotubes from satellite cells requires contact with FN, which also stimulates the rejuvenation of aging satellite cells (Lukjanenko et al., 2016). Importantly, the ability of FN to trigger myoblast regeneration, proliferation and FN matrix remodeling is linked to the expression of $\alpha 5$ and $\beta 1$ integrins (Qiao et al., 2014; Rozo et al., 2016; Taverna et al., 1998). Moreover, the FN-binding integrin stimulates proliferation and phosphorylation, which is counteracted by the cytoplasmic tail of α6 integrin, leading to α6β1-mediated adhesion to laminin and myoblast differentiation (Sastry et al., 1999). When myoblasts fuse and differentiate into myotubes, a switch to the laminin-binding α 7 subunit is observed to create α 7 β 1 integrins that associate with the dystroglycan complex to anchor myotubes to the surrounding basement membrane (Guo et al., 2006). Similarly, upon fusion of myoblasts into myotubes, the β1D integrin isoform is expressed, creating $\alpha 5\beta 1D$ and $\alpha 7\beta 1D$ subpopulations (Nawrotzki et al., 2003; van der Flier et al., 1997). One of the hallmarks of β1D integrin is its higher affinity for talins, and hence previous studies have proposed that enhanced mechanical linkage of myotubes to the ECM could be the major functional role of the β1D integrin isoform (Anthis et al., 2010; Belkin et al., 1997).

We propose in this manuscript that the differential cytoplasmic $\beta 1$ integrin tail sequences are responsible for the observed differential biological effects, assuming an equal pairing of the integrin splice forms with a given α integrin subunit (Lenter and Vestweber, 1994). However, we cannot exclude that some of the reported observations result instead from a differential α integrin subunit association, which could be induced by integrin adapter proteins recognizing specific pairs of cytoplasmic clasped (inactive) tails of the integrin heterodimers (Tseng et al., 2018). While this is an interesting hypothesis, we would like to propose that specific cytoplasmic features of $\beta 1D$ integrin cause its biological effects.

Thus, in addition to enhanced talin binding (Anthis et al., 2010; Belkin et al., 1997), \(\beta 1D \) integrin is also less prone to be modulated by phosphorylation at the inter-NPXY region (Fig. 4A). In β1A, the phosphorylation of the T788/T789 motif, or its PP2A (also known as PP2AA)-mediated dephosphorylation, induce focal adhesion disassembly or formation, respectively (Kim et al., 2004). Switching the T788/T789 motif in \(\beta 1A \) to the N788/N789 motif found in β1D created integrin-dependent adhesions insensitive to conditions that destabilized \(\beta 1 \) integrin by Ser/Thr phosphorylation. Notably, activation of CAMKII has been directly associated with phosphorylation of the TT motif and destabilization of \$1A integrin (Bouvard et al., 1998; Suzuki and Takahashi, 2003). In addition, CAMKII phosphorylation of Icap-1 (also known as ITGB1BP1) led to its activation, which then caused competition with kindlin2 for binding to \$1A integrins and subsequent integrin dissociation from focal adhesions (Brunner et al., 2011; Millon-Frémillon et al., 2013). The potential

competition between Icap-1 and kindlin2 for \$1A integrin binding is relevant as kindlin2 is critical for integrin activation (Montanez et al., 2008; Theodosiou et al., 2016). Interestingly, biochemical binding assays also revealed that mutation of the T788/ T789 motif (T788A/T789A) blocked binding of the closely related kindlin3 to GST-β1A integrin tail fusion proteins (Moser et al., 2008). Although the T788N/T789N mutations were not specifically tested in the kindlin-binding assay, kindlin3 binding to β1D integrin cytoplasmic tail was found to be reduced compared to \(\beta 1 \) A integrin (Yates et al., 2012). The reduced binding of kindlin to the β1D tail in biochemical assays, as well as the failure of C-terminal truncations of the \beta 1D tail to affect integrin recruitment to focal adhesions, indicate that kindlins are not required for the activation and function of β 1D integrin. This strongly suggests that firstly, β 1D integrin is not only independent of regulation by Ser/Thr kinases and PP2A, but is also insensitive to C-terminal β1A integrin regulators such as Icap-1 and kindlins, and secondly, that it is mainly regulated by binding of talin1 and talin2, which are critical for the function of muscles (Conti et al., 2008).

In addition to non-responsiveness to Ser/Thr phosphorylation at the inter-NPXY region (Kim et al., 2004), we also show here that paxillin is not efficiently recruited to \(\beta 1 D \) integrin-containing adhesions. Some residual recruitment of paxillin to FN-localized B1D integrincontaining adhesions in GD25 cells could be linked to residual \(\beta \) integrin binding on FN (Bachmann et al., 2018 preprint), as previously observed for high-affinity talin-binding \beta integrins (Pinon et al., 2014), or linked to a different mechanosensitive threshold. This might be explained by reduced kindlin binding to the C-terminal integrin tail (Yates et al., 2012), which could also affect the assembly of FN-fibrils (Fig. 2). Nevertheless, the delayed spreading of β1D integrinexpressing GD25 cells on FN, or their reduced proliferation, suggests that the altered recruitment of paxillin to this integrin affects intracellular signaling, while at the same time maintaining strong talin-mediated cell matrix adhesions of myotubes to tendons and basement membranes that are not prone to being affected by rises in CAMKII activity resulting from elevated intracellular Ca²⁺ levels.

Previously, we were able to dissociate the talin-mediated mechanical link of \(\beta \) integrins to F-actin from the capacity of ECM and talin-bound integrins to induce cell spreading (Pinon et al., 2014). Lack of cell spreading correlated with an absence of paxillin recruitment to mutant forms of \(\beta \) integrins, which included the Y747A mutant in the proximal NPXY motif, the talin-binding motif from PIPKIy (WDTANNPLY⁷⁴⁷KEA to WVYSPLH⁷⁴⁵YSA) (Pinon et al., 2014; Wegener et al., 2007), as well as the S752P mutant identified in a patient with Glanzman thrombastenia (Ma et al., 2008; Pinon et al., 2014). Interestingly, in the latter two cases, the Y747 sidechain critical for \beta3 integrin signaling (Petrich et al., 2007a) is either absent (Pinon et al., 2014), or the corresponding H745 inaccessible due to a tight turn of the PIPKIy sequence (Wegener et al., 2007). This situation is similar to the Y783 sidechain in \(\beta 1 \) D integrin, which is projected against the F3 domain surface of talin2, stabilized by additional β1D integrin–talin2 contacts at residue P786 (Anthis et al., 2010, 2009). We observed P786A and A786P mutations causing a switch in the adhesive and signaling behavior of β1D and β1A integrins, respectively, which could well reflect fivefold differences in affinity for talin2, therefore also changing the preferred intracellular localization of these integrins (Anthis et al., 2010), as well as the potential accessibility of the Y783 sidechain. Therefore, the localization of β1A integrin A786P mutant outside of peripheral focal adhesions could reflect a 'talin2-binding mode'. In this mode, the sidechain of Y783, and thus paxillin recruitment and cell proliferation, is affected by talin2 association, potentially modifying

the context and folding of the integrin peptide on the surface of the talin adapter protein, further confirming the critical role of talin in integrin-mediated signaling (Conti et al., 2008; Petrich et al., 2007b).

Recently, a different mechanism for paxillin recruitment to integrin-containing nascent adhesions has been proposed and shown to require binding to kindlin2 (Böttcher et al., 2017; Theodosiou et al., 2016). Moreover, kindlin and paxillin interactions were able to stabilize the activated state of αIIbβ3 integrin (Gao et al., 2017). This mechanism of paxillin-kindlins interaction would correlate with the failure of kindlins recruitment to the \(\beta \) integrin S752P mutant (Ma et al., 2008) and the respective loss in cell spreading despite its forced activation and talin colocalization in the D723A/S752P mutant (Pinon et al., 2014). Additionally, it would also correlate with the weak binding of kindlin3 to β1D integrin (Yates et al., 2012), thereby affecting paxillin recruitment and integrin signaling. However, the paxillin-binding defect of the SPLH or Y747A mutation in \(\beta \) integrin will not fit this model, since the kindlin-binding motif is not affected in these mutants (Bledzka et al., 2012; Moser et al., 2008). Similarly, the A786P mutation in β1A integrin may only slightly affect binding affinity to kindlin2, as inferred from the recent crystal structure of kindlin2 (Li et al., 2017). In a cellular context, however, kindlin2 binding could become strongly affected by adjacent high-affinity talin2 binding at the P786 residue. In fact, the crystal structure of the β1D integrin peptide bound to talin2 (Anthis et al., 2010, 2009), suggests a steric effect on the inter-NPXY residues (N788, N789), thereby affecting kindlin binding and subsequent paxillin recruitment.

Nevertheless, in all the reported paxillin-binding-deficient integrin sequences, either the modification or accessibility of the tyrosine residue in the talin-binding NPXY motif (Y747A or SPLH) or the inter-NPXY sequence is altered by proline residues. Since proline residues affect the secondary structure of the integrin peptide, it is likely that their presence either perturbs kindlin recruitment or sterically affects the recruitment of paxillin to the integrin-talin-kindlin complex. In this regard, the phenotype of the β1D integrin P786A mutation is interesting. On the one hand, the P786A mutation in β1D integrin affects the stability of the integrin within adhesions (as demonstrated using FRAP), while also correlating with a twofold reduction in biochemical interaction with talin1 (Fig. 5H), and a fivefold reduced affinity for talin2 as reported by Anthis et al. (2010). Although the reduction in talin1 binding is significant, it does not reach the low levels of binding observed in \$1A and \$3 integrin tails, which, however, recruit paxillin normally when present in focal adhesions (Fig. 5H). On the other hand, the rescue of the talin2 affinity-deficient \(\beta 1D \) integrin P786A mutant (Anthis et al., 2010) through the expression of the kindlin-binding T788/T789 motif (PNN/ATT mutant) (Moser et al., 2008) suggests that a high-affinity interaction of kindlins with the inter-NPXY motif is critical for \$1A integrin recruitment into fibrillar adhesions, as well as paxillin recruitment and integrindependent signaling in peripheral focal adhesions. How paxillin recruitment is regulated by integrin sequences such as Y747 and/or kindlins binding will require further studies (Gao et al., 2017). Nevertheless, our study provides evidence for the regulation of integrin-dependent intracellular signaling by alternative splicing. Specifically, the β1D integrin splice variant demonstrates a higher affinity for the talin2 adapter protein, but at the expense of failing to support de novo FN fiber assembly, as well as failing to induce integrin-dependent signaling. This is highly relevant for the proper mechanical function of differentiated myotubes, in which the control of myosin contractility should be uncoupled from mechanosensing mechanisms observed in other cells of the body.

MATERIALS AND METHODS

cDNA and site-directed mutagenesis

The cDNA encoding human \(\beta 1 A \) integrin was obtained from Deutsches Ressourcenzentrum fur Genomforschung GmbH (RZPD; clone ID IRATp970E0719D6). It was cloned into pCDNA3 (Invitrogen) using XbaI and EcoRI sites. Mutations were introduced by primer overlap extension and subsequently verified by automated sequencing. C-terminally tagged β1A integrin was constructed identically to the previously published β3 integrin-EGFP (Ballestrem et al., 2001) by replacing the stop codon with a PinAI- and XbaI-encoding linker that was used to insert the EGFP sequence (5'-CAGTCTAGAGACCGGTTTTCCCTCATACTTCGG-3'). The resulting SPVAT linker (-aa- in Fig. 1) was much shorter than a previously published version (-bb-, a sequence of of 18 amino acids, GGGGARRRGQA-GDPPVAT, in Fig. 1), which we received as a kind gift from Dr M. Humphries, (University of Manchester, Manchester, UK) (Parsons et al., 2008). The extracellularly tagged \$1A integrin was constructed by introducing PinAI and XhoI sites in a loop in the hybrid domain by duplicating proline at position 88 (AEGKP88EDIT), which resulted in the AEGKPVSRGPEDIT sequence (bold indicates P88 and duplicate, italics indicates inserted amino acids encoded by the restriction sites) that was used to insert the EGFP sequence (Fig. 1G) (forward: 5'-AACCGGTCTCTCG-AGGACCAGAGGATATTACTCA-3'; reverse: 5'-TCCTCGAGAGACCG-GTTTGAGCTTCTCTGCTGTTC-3'; italics indicates the nucleotides encoding the restriction sites). The β1D integrin sequence was introduced into the different \$1A integrin constructs in two steps; first by exchanging glycine with glutamine at position 778, and then by the modification of the 3' sequence of S785, using the following overlapping primers (forward: 5'-GTCCTATTAATAATTTCAAGAATCCAAACTACGGACGT-3'; reverse: 5'-TGTTCTAGATTAGAGACCAGCTTTACGTCCGTAGT-3'). The pcDNA3-based vectors were used for transient transfections of 3T3, C2C12 and GE11 cells. For stable transfections of GD25 cells, and in order to avoid an excessive, but maintain a moderate, long-term transcription in stably transfected cells, the CMV promoter of the pcDNA3 vector was replaced by a 1 kb fragment of the matrix attachment region of chicken lysozyme (MAR, kind gift from Dr Nicolas Mermod, Ecole Polytechnique Fédérale, Lausanne, Switzerland) (Girod et al., 2005; Loc and Strätling, 1988), and a 1.4 kb fragment (NheI-EcoRI) of the human β-actin promoter. Since GD25 cells are resistant to G418, the neomycin resistance gene in the modified β1A(D) integrin-containing pcDNA3 (sm-pcDNA3) was swapped for that of the puromycin gene (smppcDNA3). This same vector was also used to express the IL2 receptor alpha-β1 integrin fusion constructs, as well as the generation of puromycinresistant clones in C2C12 cells. The extracellular domain of Tac (Paulhe et al., 2009) was fused to the transmembrane and cytoplasmic domains of β1A and β1D integrins using unique BgIII and XbaI sites. Talin1–mCherry and talin2-YPet constructs were previously published and the latter a kind gift from Dr Carsten Grashoff, University of Münster, Münster, Germany) (Austen et al., 2015; Rahikainen et al., 2017). DNA sequence analysis was performed for all constructs and mutants to ensure error-free amplification and correct base replacement.

Cell culture, transient and stable transfections

Mouse C2C12 myoblast cell (ATCC, CRL-1772), NIH 3T3 fibroblast cells (ATCC, CRL-1658), as well as \$1 integrin-deficient GD25 and GE11 cells as described in Fassler et al. (1995) (a kind gift from Dr Reinhard Faessler, Max Planck Institute for Biochemistry, Martinsried, Germany) were grown in DME containing 10% FCS, glutamine and antibiotics, as previously described (Ballestrem et al., 2001). For 3T3 and GD25 cells, transfections were performed with Jet PeI (Polyplus Transfection) according to the manufacturer's recommendation. For C2C12 and GE11 cells, electroporation was performed using a Microporator from Axonlab following the guidelines from the manufacturer. For selection of stably transfected GD25 cells, medium was supplemented with puromycin, and cells subsequently sorted using FACS with gating for surface expression of human β1A, or β1D integrin, as detected by reactivity with anti-human CD29 (\$1 integrin) monoclonal antibody (mAb) (1:500, clone Ts2/16, BioLegend). Jet Prime was used for the transient transfection of C2C12 cells with talin1/2, Tac-β1A

integrin and Tac- β 1D integrin constructs, according to the manufacturer's recommendation (Polyplus Transfection).

Antibodies and immunofluorescence

Cells grown in complete medium were fixed with 4% PFA in PBS for 10 min, permeabilized, and blocked in 0.1% Triton X-100 and 1% BSA in PBS for 30 min. Mouse mAbs raised against vinculin (1:600, V9131, Sigma-Aldrich), paxillin (1:1000, clone 349, lot no. 610051, BD Transduction Laboratories), Tac epitope (1:500, clone 7G7, Merck-Millipore), phospho-tyrosine (1:500, 4G10 Platinum, Millipore); rabbit-polyclonal antibody raised against fibronectin (1:500, clone 1801, a gift from Dr Matthias Chiquet, Zahnmedizinische Kliniken, Bern, Switzerland) and rat anti-mouse CD29 mAb (1:200, clone 9EG7, 553715, BD Transduction Laboratories) that detects activated β1 integrin were applied in 1% BSA-PBS for 1 h. After washing in blocking solution, Texas Red-conjugated goat anti-mouse (1:1000, 115-075-003, Jackson ImmunoResearch Laboratories), Cy5-conjugated goat anti-rabbit (paired with anti-fibronectin) (1:400, 111-175-144, Jackson ImmunoResearch Laboratories) or Texas Red-conjugated goat anti-rat (1:400, 112-075-143, Jackson ImmunoResearch Laboratories) secondary antibodies were applied for 1 h and subsequently washed as above. F-actin was detected with Texas Redphalloidin (1:2000, MP00354, Invitrogen). Preparations were stored in PBS and images were collected at room temperature using a 63×1.40 NA objective on an LSM510 inverted microscope. In addition, background and contrast were adjusted using the 'Level' command in Photoshop (Adobe).

TIRF microscopy

Intra-objective TIRF microscopy was performed using an inverted microscope (Axiovert 100M; Carl Zeiss, Inc.) equipped with a combined epifluorescence/ TIRF adapter (TILL Photonics) and a $100\times$ NA 1.45 objective (Carl Zeiss, Inc.). EGFP fusion proteins were excited with the 488-nm line of a 150-mW argon-ion laser (Reliant 150 m; Laser Physics), and red dyes were excited with the 535-nm line of a 20-mW diode laser (Compass 215M-20; Coherent, Inc.). Laser output at the end of the optical fiber was set to 5 mW each, to assure equal illumination of biological samples with the blue or green laser light. Openlab software (PerkinElmer) controlled image capture by a 12-bit charge-coupled device camera (Orca 9742-95; Hamamatsu Photonics) as well as the operation of the laser shutters and microscope. The background and contrast were adjusted using the 'Level' command in Photoshop (Adobe).

Live cell imaging and FRAP

Cells were cultured in FN-coated glass-bottom dishes for 24 h in complete culture medium prior to analysis. Medium was replaced by F12 medium containing glutamine, antibiotics and 10% FCS prior to live cell imaging and FRAP analysis. FRAP experiments with NIH 3T3 and C2C12 cells were performed at 37°C on an LSM510 inverted microscope equipped with a heated stage and CO_2 control essentially as described previously (Ballestrem et al., 2001; Wehrle-Haller, 2007). To reduce loss of fluorescence due to bleaching during the recovery period, we reduced the laser power of the 488-nm line to 0.5% at a maximal laser output of 50%. To improve light collection, the pin hole was partially opened (to 200 μm). To ensure maintenance of the focus during the recovery period, an IRM image was recorded simultaneously. Time-lapse analysis was performed using the same settings and image scans were performed every 40 s.

For stably transfected GD25 cells, culture and live-cell imaging conditions were identical to those described as above, but measurements were performed on a Nikon A1r inverted confocal microscope equipped with an autofocus module and a 60× oil objective NA 1.4, pinhole of 2.3 (CFI Plan Apochromat VC WD:0.13 mm), at zoom 4, and with a 488 nm 50 mW laser at 37°C, 10% CO₂. For FRAP experiments in GD25 cells, 12-bit confocal images were acquired every 20 s over 17 min. Gray level intensities of bleaching zones, as well as of non-bleached adhesion sites to compensate for bleaching during recovery period, and empty control background areas were analyzed by ImageJ and values were treated essentially as described previously (Wehrle-Haller, 2007).

FACS

Stably transfected GD25 cells were detached with trypsin/EDTA, blocked in culture medium and incubated with primary antibodies, rat anti-mouse

CD29 (1:200, clone 9EG7, 553715, BD Transduction Laboratories) or antihuman CD29 (β 1 integrin) (1:500, clone Ts2/16, 303009, BioLegend), for 45 min on ice. Cells were washed and re-suspended in DMEM and incubated with the secondary antibody, goat anti-mouse Phycoerythrin (PE) or goat anti-rat PE for 30 min on ice. Cells were washed twice and re-suspended in PBS for the FACS analysis. FACS was performed with a BD FACSAria II instrument (selecting between 10,000 and 100,000 cells for reseeding).

Substrate coating and microcontact printing with extracellular matrix proteins

For spreading experiments on defined protein substrates, glass coverslips were coated for 1 h at room temperature with purified horse serum-derived FN (a gift from Dr Matthias Chiquet), or EHS tumor-derived laminin-111 (a gift from Dr Jürgen Engel, Biocenter, Basel, Switzerland) diluted in PBS at the indicated concentrations, followed by washing and blocking of the coated surfaces with 1 mg/ml human serum albumin (Sigma-Aldrich).

Silicone stamps for microcontact printing of differential substrates were produced as previously described (Lehnert et al., 2004). Binary choice substrates were produced with human plasma FN (Sigma-Aldrich, F2006 or Millipore, FC010) and human plasma VN (Sigma-Aldrich, V8379). Silicone stamps were incubated for 10 min with a solution of 5 µg/ml FN and 45 µg/ml heat-inactivated FN in PBS. Alexa Fluor 647-labeled FN was produced with the A20173 fluorescence labeling kit, (Thermo Fisher) according to the manufacturer's recommendation. Labeled FN was diluted (1.5 μ l in 100 μ l of total FN solution) and then used for the stamping method to visualize the FN pattern. After nitrogen drying, the stamp was pressed onto a glass cover slip for 10 min before it was released. Next, the pattern was covered with VN at a concentration of 5 µg/ml in PBS for 1 h at room temperature. Heat-inactivated FN was produced by heating FN for 30 min to 90°C and was added to block VN adsorption in the stamped area. Cells do not spread on heat-inactivated FN. After the final incubation step, patterns were washed with PBS and used directly for cell seeding. Detachment from culture flasks was stopped with trypsin inhibitor (Sigma-Aldrich) and cells were seeded in DMEM without FCS if not stated otherwise.

Automated and manual integrin adhesion length measurements

Integrin-transfected cells were incubated for 8 h on FN-coated glass coverslips and fixed for 10 min in 4% PFA/PBS. TIRF images were taken in PBS. Adhesion length measurements were obtained from 12-bit images after selection of the cell area and background subtraction, using MetaMorph software (Molecular Devices). Integrin adhesions were identified with the 'angiogenesis tool' and subsequently skeletonized to one pixel width to obtain the adhesion length measurements of individual adhesions. The average adhesion length per cell was calculated from all the adhesions identified in one cell and the measurement performed on at least 20 cells per experiment, which were repeated four times.

The adhesion length distribution analysis was performed manually on TIRF images of GFP- $\beta 1$ integrin fluorescence, with the help of the line tool in ImageJ. Each adhesion length distribution profile was grouped into decile borders and these decile values were averaged over one experiment (n=8 cells, 3 experiments). To test how much influence the choice of images for quantification and personal interpretation of adhesion lengths would have, two different investigators independently quantified the cell adhesion length distributions of different pictures from the same experiment. Both investigators obtained the same trends for adhesion length distributions and mean values. These results let us conclude that adhesion length distributions measurements can be reproduced and image choice does not alter the result.

Recombinant protein purification and Octet biosensor analysis

Purification of GST–β1 integrin tail chimeras and His₆-tagged talin1 head domain (residues 1–406) were performed as described previously (Pinon et al., 2014). In brief, proteins were produced in *E. coli* BL-21-Star cells (Invitrogen) and induced with 1 mM IPTG for 5 h at 37°C, then lysed by homogenization (Emulsiflex C3, Avestin Inc.) in PBS containing protease inhibitor cocktail. GST-tagged proteins were purified on Glutathione Sepharose (GE Healthcare 4 Fast Flow), detached in 50 mM Tris-HCl,

containing 20 mM reduced glutathione (pH 8) and dialyzed into 50 mM sodium phosphate buffer (150 mM NaCl, pH 7.2) before analysis by SDS-PAGE, Coomassie Blue staining and concentration UV/Vis absorption analysis. The His₆-tagged talin1 head domain lysates were generated in 20 mM sodium phosphate buffer (1 M NaCl, 20 mM imidazole, pH 7.4) and purified on HisTrap FF affinity columns (GE Healthcare) prior to elution with a linear imidazole gradient 0–700 mM. Eluted fractions were further purified by cation exchange chromatography using HiTrap SP FF columns (GE Healthcare), and eluted with a linear NaCl gradient prior to analysis of purity and concentration as mentioned for the GST chimeras.

Biosensor analysis was performed on a Fortebio Octet RED384 instrument at 25°C and stirring speed of 1000 rpm, using Ni-NTA sensors. Sensors were pre-wetted with buffer (50 mM NaH₂PO₄, 150 mM NaCl pH 7.2) in order to get baseline prior to immobilization. Samples or buffers were pipetted either into 96- or 384-well plates at a volume of 200 µl or 80 µl per well, respectively. Sensors were chemically activated by immersing them in 0.05 M EDC [1-ethyl-3-(3-dimethylaminopropyl) carbodiimide] and 0.1 M NHS (N-hydroxysuccinimide) in H₂O for 100 s. Talin1 head domain (50 μg/ml) was immobilized on the sensor's surface for 300 s. The excess NHS esters were quenched by 1 M ethanolamine pH 8.5 for 100 s. Serially diluted GST-β1 integrin tail chimeras were then applied on the talin1-coated sensors in concentrations of 20, 80, 320, 1250 and 5000 nM to obtain the relative affinity of integrin-GST to talin1. The binding of each concentration of integrin-GST to the sensor was measured for 300 s before moving the sensor into a well containing higher integrin-GST concentration. GST alone was used as negative control with the same conditions. In data analysis, the GST control response signal was subtracted from the measured binding response.

Super-resolution structured illumination microscopy and image analysis

Super-resolution structured illumination microscopy (SR-SIM) imaging was performed on a non-serial Zeiss Elyra PS.1 microscope with a 63×1.4 NA oil-immersion objective and an Andor iXon EMCCD camera. The grid for SR-SIM was rotated three times and shifted five times leading to 15 frames raw data out of which a final SR-SIM image was calculated with the structured illumination package of ZEN software (Zeiss). Values for calculation were selected for best resolution without causing image artifacts. Channels were aligned using a correction file that was generated by measuring channel misalignment of fluorescent tetraspecs (Thermo Fisher, T7280). Colocalization was analyzed with the Fiji software package (Schindelin et al., 2015). Colocalization to FN was quantified by measuring Mander's coefficient of thresholded images by using the Fiji plugin JACoP (Bolte and Cordelières, 2006).

Cell spreading analysis

Stably transfected $\beta 1$ integrin-expressing GD25 cells were plated for 5 h on $10\,\mu g/ml$ FN-coated coverslips in DMEM containing 10% FCS. Subsequent time-lapse videos were started and phase-contrast pictures were taken every 5 min with a $10\times$ long-distance objective on a Zeiss-Axiovert 100M microscope at a constant temperature of $37^{\circ}C$ and 10% CO $_{2}$ levels. For image analysis and detection of cell area, the cell borders were defined by the threshold tool in ImageJ and cell area and perimeter subsequently quantified.

Pearson correlation of integrins and paxillin

TIRF images of GD25 cells stably transfected with GFP-tagged $\beta 1$ integrin were acquired after overnight culture on FN-coated glass coverslips. Cells were fixed, permeabilized and stained with anti-paxillin antibody (1:1000, clone 349, lot number 610051, BD Transduction Laboratories) and Alexa Fluor 555 goat anti-mouse secondary antibody (1:1000, A32727, Thermo Fisher). Pairs of images were analyzed in ImageJ using the co-localization module to evaluate the Pearson correlation coefficient of 20 cells per data point.

BRDU incorporation and cell proliferation tests

Stably transfected and FACS-sorted GD25 cells were plated for $6\,h$ in medium containing 5% FBS on glass coverslips, previously coated with $10\,\mu\text{g/ml}$ of FN for 1 h at room temperature. The serum content of the

medium was then reduced to 1% for 20 h and then incubated for 4 h in the same medium containing BRDU, in concentrations according to the manufacturer's recommendation. Cells were fixed and stained with DAPI and anti-BRDU antibody using a commercial BRDU-labeling kit (1:100, 11296736001, Merck). Five randomly selected areas were imaged with a 10^{\times} objective and percentage of BRDU-expressing nuclei manually counted from a total of 250–500 cells per condition.

Proliferation of GD25 cell lines stably transfected with GFP–β1A integrin or GFP–β1D integrin was measured with a xCELLigence system (ACEA Biosciences Inc.). 15,000 cells of the respective cell lines were applied to specialized electrode-coated wells from ACEA Biosciences that allowed impedance measurements as a proxy for cell adhesion and increase in cell number. Impedance values were corrected for baseline levels of the medium and were converted to arbitrary units by the system software for comparison of different conditions. Experiments were performed with duplicated wells and in culture medium with 10% FCS. Impedance was measured every 15 min for 75 h and is shown as mean of three independent experiments.

Spinning disc analysis

Application of shear stress and subsequent data analysis was performed with a spinning disc device, as previously described (Boettiger, 2007; Tabone-Eglinger et al., 2014). β1 integrin-deficient GE11 cells were transiently cotransfected with GFP-tagged \$1A integrin and DSred2 red fluorescent protein (to identify integrin-transfected cells), both in pcDNA3 vectors, and plated for different times on FN-coated round coverslips. Coverslips were then mounted in the spinning disc device, spun with the spinning disc device and shear stress was applied in PBS containing Ca²⁺ and Mg²⁺ for 5 min at room temperature. Coverslips were then fixed and mounted in Fluoromount (Sigma-Aldrich). Automated red fluorescent protein and phase-contrast images were taken with an inverted Nikon microscope integrated into an ImageXpress Micro High Content Screening System (Molecular Devices). Counting and determination of the radial position of cells was performed with the MetaMorph software (Molecular Devices). Final plotting of normalized cell density and T₅₀ determination was performed with Prism6 (GraphPad Software, Inc.).

To reduce the influence of endogenous $\alpha\nu\beta3$ integrin expressed in GE11 cells, non-transfected GE11 cells were first incubated in the presence of various concentrations of the $\beta3$ integrin inhibitor S-36578-2 obtained as a gift from Dr Gordon C. Tucker, Servier, Croissy-sur-Seine, France), to determine conditions in which non-transfected GE11 cell adhesion to FN-coated coverslips was minimal. We then selected 400 nM inhibitor for 30 and 60 min of cell incubation with the coated coverslips prior to shear stress application.

Statistical analysis

Experiments were performed at least in triplicates and the mean \pm s.e.m. were determined. Paired Student's *t*-test (for direct sample comparison), or one-way ANOVA analysis (for comparison of multiple samples) were performed with Excel (Microsoft) and GraphPad Prism. Significant differences were assumed when P<0.05. If not specifically mentioned P-values were indicated as **P<0.01, ****P<0.001 and ****P<0.0001.

Acknowledgements

We would like to thank Dr G. Kastberger for help in the adhesion velocity analysis and the members of the Bioimaging core facility of the Centre Médical Universitaire for help in microscopy and image analysis. Biocenter Finland is acknowledged for infrastructure support.

Competing interests

The authors declare no competing or financial interests.

Author contributions

Conceptualization: M.S.-R., B.K., M. Bachmann, D. Boettiger, D. Bouvard, M. Bastmeyer, V.P.H., B.W.-H.; Methodology: M.S.-R., B.K., M. Bachmann, L.A., K.F., M.-C.J., D. Boettiger, M. Bastmeyer, V.P.H., B.W.-H.; Formal analysis: M.S.-R., B.K., M. Bachmann, B.W.-H.; Investigation: M.S.-R., B.K., M. Bachmann, B.W.-H.; C.J., D. Boettiger; Resources: D. Bouvard; Data curation: M. Bachmann, B.W.-H.; Writing - original draft: B.W.-H.; Writing - review & editing: M. Bachmann, V.P.H., B.W.-H.; Visualization: M. Bastmeyer, B.W.-H.; Supervision: D. Boettiger, V.P.H., B.W.-H.; Project administration: B.W.-H.; Funding acquisition: B.W.-H.

Funding

We would like to thank the Swiss Foundation for Research on Muscle Diseases (Stiftung für die Erforschung der Muskelkrankheiten) for their support of M.S.-R. and B.K. Additional funding for the project was provided by grants from the Swiss National Science Foundation (Schweizerischer Nationalfonds zur Förderung der Wissenschaftlichen Forschung) to B.W.-H. (31003A 146283 and 31003A 166384). Academy of Finland is acknowledged for financial support of the research in the Hytönen group.

Supplementary information

Supplementary information available online at http://jcs.biologists.org/lookup/doi/10.1242/jcs.224493.supplemental

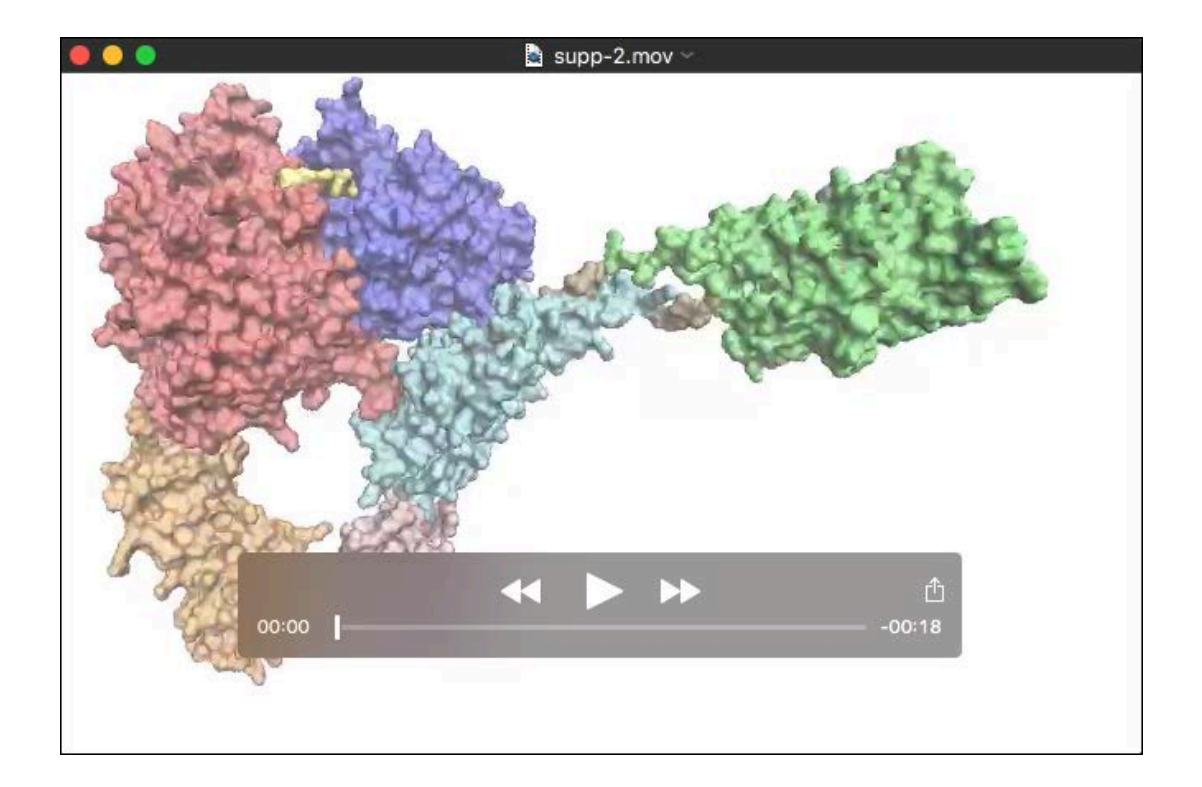
References

- Anthis, N. J., Wegener, K. L., Ye, F., Kim, C., Goult, B. T., Lowe, E. D., Vakonakis, I., Bate, N., Critchley, D. R., Ginsberg, M. H. et al. (2009). The structure of an integrin/talin complex reveals the basis of inside-out signal transduction. *EMBO J.* 28, 3623-3632. doi:10.1038/emboj.2009.287
- Anthis, N. J., Wegener, K. L., Critchley, D. R. and Campbell, I. D. (2010). Structural diversity in integrin/talin interactions. Structure 18, 1654-1666. doi:10. 1016/i.str.2010.09.018
- Austen, K., Ringer, P., Mehlich, A., Chrostek-Grashoff, A., Kluger, C., Klingner, C., Sabass, B., Zent, R., Rief, M. and Grashoff, C. (2015). Extracellular rigidity sensing by talin isoform-specific mechanical linkages. *Nat. Cell Biol.* 17, 1597-1606. doi:10.1038/ncb3268
- Bachmann, M., Schäfer, M., Mykuliak, V., Ripamonti, M., Heiser, L., Weißenbruch, K., Krübel, S., Franz, C. M., Hytönen, V., Wehrle-Haller, B. and Bastmeyer, M. (2018). Ligand binding promiscuity of αVβ3 integrin is enlarged in response to mechanical force. *bioRxiv* 200493-1606. doi:10.1101/200493
- Ballestrem, C., Hinz, B., Imhof, B. A. and Wehrle-Haller, B. (2001). Marching at the front and dragging behind: differential alphaVbeta3 integrin turnover regulates focal adhesion behavior. J. Cell Biol. 155, 1319-1332. doi:10.1083/jcb.200107107
- Baudoin, C., Goumans, M.-J., Mummery, C. and Sonnenberg, A. (1998). Knockout and knockin of the beta1 exon D define distinct roles for integrin splice variants in heart function and embryonic development. *Genes Dev.* 12, 1202-1216. doi:10.1101/gad.12.8.1202
- Bazzoni, G., Shih, D. T., Buck, C. A. and Hemler, M. E. (1995). Monoclonal antibody 9EG7 defines a novel beta 1 integrin epitope induced by soluble ligand and manganese, but inhibited by calcium. *J. Biol. Chem.* **270**, 25570-25577. doi:10.1074/jbc.270.43.25570
- Belkin, A. M. and Retta, S. F. (1998). beta1D integrin inhibits cell cycle progression in normal myoblasts and fibroblasts. *J. Biol. Chem.* **273**, 15234-15240. doi:10. 1074/jbc.273.24.15234
- Belkin, A. M., Zhidkova, N. I., Balzac, F., Altruda, F., Tomatis, D., Maier, A., Tarone, G., Koteliansky, V. E. and Burridge, K. (1996). Beta 1D integrin displaces the beta 1A isoform in striated muscles: localization at junctional structures and signaling potential in nonmuscle cells. J. Cell Biol. 132, 211-226. doi:10.1083/jcb.132.1.211
- Belkin, A. M., Retta, S. F., Pletjushkina, O. Y., Balzac, F., Silengo, L., Fassler, R., Koteliansky, V. E., Burridge, K. and Tarone, G. (1997). Muscle beta1D integrin reinforces the cytoskeleton-matrix link: modulation of integrin adhesive function by alternative splicing. *J. Cell Biol.* **139**, 1583-1595. doi:10.1083/jcb.139.6.1583
- Bledzka, K., Liu, J., Xu, Z., Perera, H. D., Yadav, S. P., Bialkowska, K., Qin, J., Ma, Y.-Q. and Plow, E. F. (2012). Spatial coordination of kindlin-2 with talin head domain in interaction with integrin beta cytoplasmic tails. *J. Biol. Chem.* 287, 24585-24594. doi:10.1074/ibc.M111.336743
- Boettiger, D. (2007). Quantitative measurements of integrin-mediated adhesion to extracellular matrix. *Methods Enzymol.* 426, 1-25. doi:10.1016/S0076-6879(07)26001-X
- Bolte, S. and Cordelières, F. P. (2006). A guided tour into subcellular colocalization analysis in light microscopy. *J. Microsc.* **224**, 213-232. doi:10.1111/j.1365-2818.
- Böttcher, R. T., Veelders, M., Rombaut, P., Faix, J., Theodosiou, M., Stradal, T. E., Rottner, K., Zent, R., Herzog, F. and Fässler, R. (2017). Kindlin-2 recruits paxillin and Arp2/3 to promote membrane protrusions during initial cell spreading. *J. Cell Biol.* **216**, 3785-3798. doi:10.1083/jcb.201701176
- Bouvard, D., Molla, A. and Block, M. R. (1998). Calcium/calmodulin-dependent protein kinase II controls alpha5beta1 integrin-mediated inside-out signaling.
- Brunner, M., Millon-Frémillon, A., Chevalier, G., Nakchbandi, I. A., Mosher, D., Block, M. R., Albigès-Rizo, C. and Bouvard, D. (2011). Osteoblast mineralization requires beta1 integrin/ICAP-1-dependent fibronectin deposition. *J. Cell Biol.* **194**, 307-322. doi:10.1083/jcb.201007108
- Bunch, T. A., Helsten, T. L., Kendall, T. L., Shirahatti, N., Mahadevan, D., Shattil, S. J. and Brower, D. L. (2006). Amino acid changes in Drosophila alphaPS2betaPS integrins that affect ligand affinity. J. Biol. Chem. 281, 5050-5057. doi:10.1074/jbc.M508550200

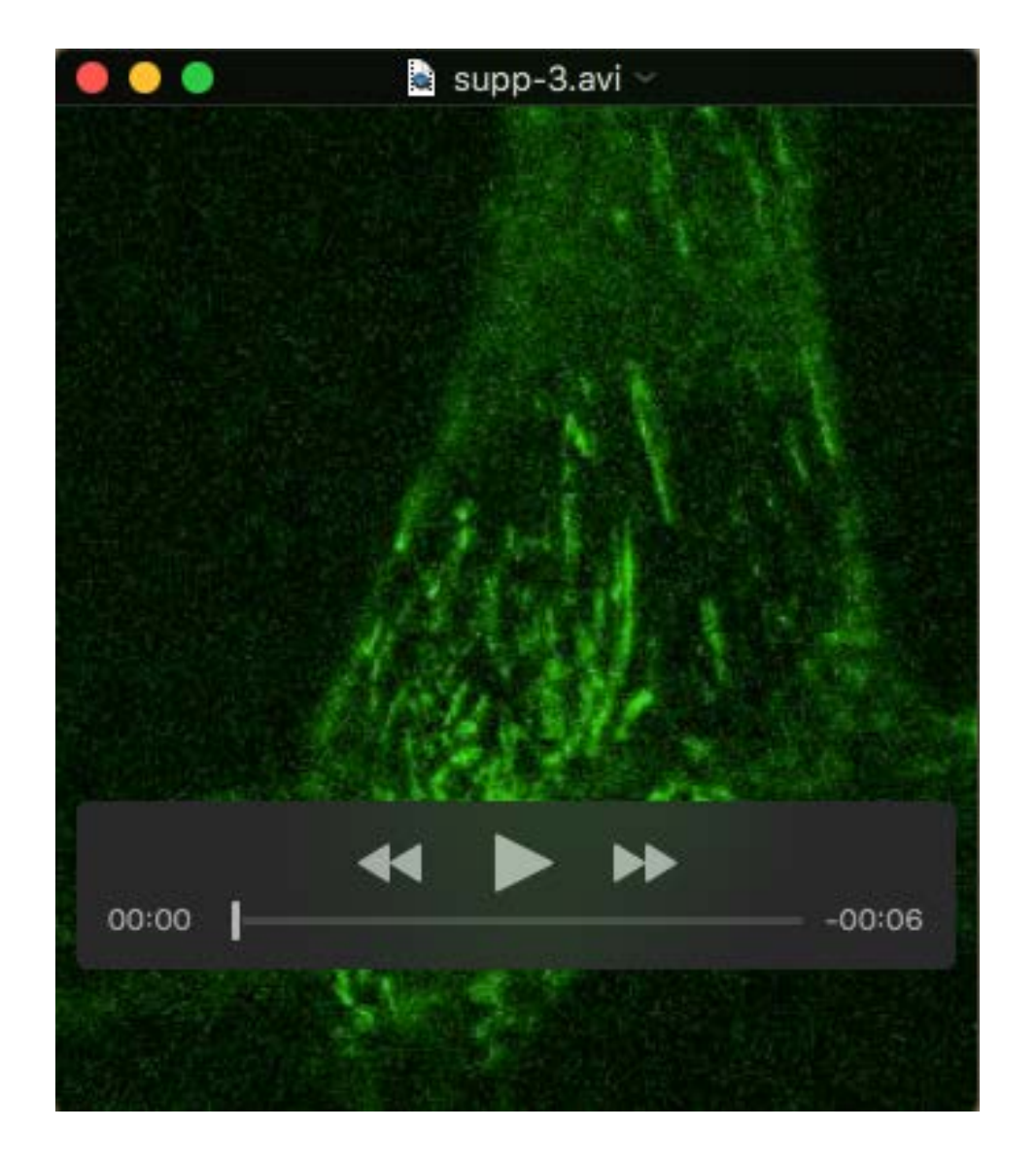
- Cachaco, A. S., Chuva, S. M., de Sousa Lopes, Kuikman, I., Bajanca, F., Abe, K., Baudoin, C., Sonnenberg, A., Mummery, C. L. and Thorsteinsdottir, S. (2003). Knock-in of integrin beta 1D affects primary but not secondary myogenesis in mice. *Development* 130, 1659-1671. doi:10.1242/dev.00394
- Caswell, P. T., Spence, H. J., Parsons, M., White, D. P., Clark, K., Cheng, K. W., Mills, G. B., Humphries, M. J., Messent, A. J., Anderson, K. I. et al. (2007). Rab25 associates with alpha5beta1 integrin to promote invasive migration in 3D microenvironments. *Dev. Cell* 13, 496-510. doi:10.1016/j.devcel.2007.08.012
- Chen, L. B. (1977). Alteration in cell surface LETS protein during myogenesis. Cell. 10, 393-400. doi:10.1016/0092-8674(77)90026-5
- Chevallier, A. (1979). Role of the somitic mesoderm in the development of the thorax in bird embryos. II. Origin of thoracic and appendicular musculature. J. Embryol. Exp. Morphol. 49, 73-88.
- Chiquet, M., Eppenberger, H. M. and Turner, D. C. (1981). Muscle morphogenesis: evidence for an organizing function of exogenous fibronectin. *Dev. Biol.* **88**, 220-235. doi:10.1016/0012-1606(81)90166-4
- Cluzel, C., Saltel, F., Lussi, J., Paulhe, F., Imhof, B. A. and Wehrle-Haller, B. (2005). The mechanisms and dynamics of (alpha)v(beta)3 integrin clustering in living cells. *J. Cell Biol.* **171**, 383-392. doi:10.1083/jcb.200503017
- Conti, F. J., Felder, A., Monkley, S., Schwander, M., Wood, M. R., Lieber, R., Critchley, D. and Muller, U. (2008). Progressive myopathy and defects in the maintenance of myotendinous junctions in mice that lack talin 1 in skeletal muscle. *Development* 135, 2043-2053. doi:10.1242/dev.015818
- de Almeida, P. G., Pinheiro, G. G., Nunes, A. M., Gonçalves, A. B. and Thorsteinsdóttir, S. (2016). Fibronectin assembly during early embryo development: a versatile communication system between cells and tissues. *Dev. Dyn.* **245**, 520-535. doi:10.1002/dvdy.24391
- Egervari, K., Potter, G., Guzman-Hernandez, M. L., Salmon, P., Soto-Ribeiro, M., Kastberger, B., Balla, T., Wehrle-Haller, B. and Kiss, J. Z. (2016). Astrocytes spatially restrict VEGF signaling by polarized secretion and incorporation of VEGF into the actively assembling extracellular matrix. *Glia* 64, 440-456. doi:10.1002/glia.22939
- Fassler, R., Pfaff, M., Murphy, J., Noegel, A. A., Johansson, S., Timpl, R. and Albrecht, R. (1995). Lack of beta 1 integrin gene in embryonic stem cells affects morphology, adhesion, and migration but not integration into the inner cell mass of blastocysts. *J. Cell Biol.* **128**, 979-988. doi:10.1083/jcb.128.5.979
- Fitzpatrick, P., Shattil, S. J. and Ablooglu, A. J. (2014). C-terminal COOH of integrin beta1 is necessary for beta1 association with the kindlin-2 adapter protein. *J. Biol. Chem.* **289**, 11183-11193. doi:10.1074/jbc.M113.535369
- Fornaro, M. and Languino, L. R. (1997). Alternatively spliced variants: a new view of the integrin cytoplasmic domain. *Matrix Biol.* **16**, 185-193. doi:10.1016/S0945-053X(97)90007-X
- Friedland, J. C., Lee, M. H. and Boettiger, D. (2009). Mechanically activated integrin switch controls alpha5beta1 function. Science 323, 642-644. doi:10.1126/ science.1168441
- Gao, J., Huang, M., Lai, J., Mao, K., Sun, P., Cao, Z., Hu, Y., Zhang, Y., Schulte, M. L., Jin, C. et al. (2017). Kindlin supports platelet integrin alphallbbeta3 activation by interacting with paxillin. J. Cell Sci. 130, 3764-3775. doi:10.1242/jcs.205641
- Girod, P.-A., Zahn-Zabal, M. and Mermod, N. (2005). Use of the chicken lysozyme 5' matrix attachment region to generate high producer CHO cell lines. *Biotechnol. Bioeng.* **91**, 1-11. doi:10.1002/bit.20563
- Guo, C., Willem, M., Werner, A., Raivich, G., Emerson, M., Neyses, L. and Mayer, U. (2006). Absence of alpha 7 integrin in dystrophin-deficient mice causes a myopathy similar to Duchenne muscular dystrophy. *Hum. Mol. Genet.* 15, 989-998. doi:10.1093/hmg/ddl018
- Huet-Calderwood, C., Rivera-Molina, F., Iwamoto, D. V., Kromann, E. B., Toomre, D. and Calderwood, D. A. (2017). Novel ecto-tagged integrins reveal their trafficking in live cells. *Nat. Commun.* 8, 570. doi:10.1038/s41467-017-00646-w
- Humphries, J. D., Byron, A. and Humphries, M. J. (2006). Integrin ligands at a glance. *J. Cell Sci.* **119**, 3901-3903. doi:10.1242/jcs.03098
- Hynes, R. O. (2002). Integrins: bidirectional, allosteric signaling machines. Cell 110, 673-687. doi:10.1016/S0092-8674(02)00971-6
- Kendall, T., Mukai, L., Jannuzi, A. L. and Bunch, T. A. (2011). Identification of integrin beta subunit mutations that alter affinity for extracellular matrix ligand. J. Biol. Chem. 286, 30981-30993. doi:10.1074/jbc.M111.254797
- Kim, S.-M., Kwon, M. S., Park, C. S., Choi, K.-R., Chun, J.-S., Ahn, J. and Song, W. K. (2004). Modulation of Thr phosphorylation of integrin beta1 during muscle differentiation. J. Biol. Chem. 279, 7082-7090. doi:10.1074/jbc.M311581200
- LaFlamme, S. E., Thomas, L. A., Yamada, S. S. and Yamada, K. M. (1994). Single subunit chimeric integrins as mimics and inhibitors of endogenous integrin functions in receptor localization, cell spreading and migration, and matrix assembly. J. Cell Biol. 126, 1287-1298. doi:10.1083/jcb.126.5.1287
- Laukaitis, C. M., Webb, D. J., Donais, K. and Horwitz, A. F. (2001). Differential dynamics of alpha 5 integrin, paxillin, and alpha-actinin during formation and disassembly of adhesions in migrating cells. *J. Cell Biol.* 153, 1427-1440. doi:10. 1083/jcb.153.7.1427
- Leduc, C., Si, S., Gautier, J., Soto-Ribeiro, M., Wehrle-Haller, B., Gautreau, A., Giannone, G., Cognet, L. and Lounis, B. (2013). A highly specific gold nanoprobe for live-cell single-molecule imaging. *Nano Lett.* 13, 1489-1494. doi:10.1021/nl304561g

- Lehnert, D., Wehrle-Haller, B., David, C., Weiland, U., Ballestrem, C., Imhof, B. A. and Bastmeyer, M. (2004). Cell behaviour on micropatterned substrata: limits of extracellular matrix geometry for spreading and adhesion. *J. Cell Sci.* 117, 41-52. doi:10.1242/jcs.00836
- Lenter, M. and Vestweber, D. (1994). The integrin chains beta 1 and alpha 6 associate with the chaperone calnexin prior to integrin assembly. J. Biol. Chem. 269, 12263-12268.
- Lenter, M., Uhlig, H., Hamann, A., Jeno, P., Imhof, B. and Vestweber, D. (1993).
 A monoclonal antibody against an activation epitope on mouse integrin chain beta 1 blocks adhesion of lymphocytes to the endothelial integrin alpha 6 beta 1. *Proc. Natl. Acad. Sci. USA* 90, 9051-9055. doi:10.1073/pnas.90.19.9051
- Li, H., Deng, Y., Sun, K., Yang, H., Liu, J., Wang, M., Zhang, Z., Lin, J., Wu, C., Wei, Z. et al. (2017). Structural basis of kindlin-mediated integrin recognition and activation. *Proc. Natl. Acad. Sci. USA* **114**, 9349-9354. doi:10.1073/pnas.1703064114
- Loc, P. V. and Strätling, W. H. (1988). The matrix attachment regions of the chicken lysozyme gene co-map with the boundaries of the chromatin domain. *EMBO J.* **7**, 655-664. doi:10.1002/j.1460-2075.1988.tb02860.x
- Lukjanenko, L., Jung, M. J., Hegde, N., Perruisseau-Carrier, C., Migliavacca, E., Rozo, M., Karaz, S., Jacot, G., Schmidt, M., Li, L. et al. (2016). Loss of fibronectin from the aged stem cell niche affects the regenerative capacity of skeletal muscle in mice. *Nat. Med.* 22, 897-905. doi:10.1038/nm.4126
- Ma, Y.-Q., Qin, J., Wu, C. and Plow, E. F. (2008). Kindlin-2 (Mig-2): a co-activator of beta3 integrins. J. Cell Biol. 181, 439-446. doi:10.1083/jcb.200710196
- Margadant, C., Kreft, M., de Groot, D.-J., Norman, J. C. and Sonnenberg, A. (2012). Distinct roles of talin and kindlin in regulating integrin alpha5beta1 function and trafficking. *Curr. Biol.* 22, 1554-1563. doi:10.1016/j.cub.2012.06.060
- Maubant, S., Saint-Dizier, D., Boutillon, M., Perron-Sierra, F., Casara, P. J., Hickman, J. A., Tucker, G. C. and Van Obberghen-Schilling, E. (2006). Blockade of alpha v beta3 and alpha v beta5 integrins by RGD mimetics induces anoikis and not integrin-mediated death in human endothelial cells. *Blood* 108, 3035-3044. doi:10.1182/blood-2006-05-023580
- Millon-Frémillon, A., Brunner, M., Abed, N., Collomb, E., Ribba, A.-S., Block, M. R., Albigès-Rizo, C. and Bouvard, D. (2013). Calcium and calmodulin-dependent serine/threonine protein kinase type II (CaMKII)-mediated intramolecular opening of integrin cytoplasmic domain-associated protein-1 (ICAP-1alpha) negatively regulates beta1 integrins. J. Biol. Chem. 288, 20248-20260. doi:10.1074/jbc.M113.455956
- Montanez, E., Ussar, S., Schifferer, M., Bosl, M., Zent, R., Moser, M. and Fassler, R. (2008). Kindlin-2 controls bidirectional signaling of integrins. *Genes Dev.* 22, 1325-1330. doi:10.1101/gad.469408
- Moser, M., Nieswandt, B., Ussar, S., Pozgajova, M. and Fässler, R. (2008). Kindlin-3 is essential for integrin activation and platelet aggregation. *Nat. Med.* 14, 325-330. doi:10.1038/nm1722
- Nawrotzki, R., Willem, M., Miosge, N., Brinkmeier, H. and Mayer, U. (2003). Defective integrin switch and matrix composition at alpha 7-deficient myotendinous junctions precede the onset of muscular dystrophy in mice. *Hum. Mol. Genet.* **12**, 483-495. doi:10.1093/hmg/ddg047
- Pankov, R., Cukierman, E., Katz, B.-Z., Matsumoto, K., Lin, D. C., Lin, S., Hahn, C. and Yamada, K. M. (2000). Integrin dynamics and matrix assembly: tensin-dependent translocation of alpha(5)beta(1) integrins promotes early fibronectin fibrillogenesis. J. Cell Biol. 148, 1075-1090. doi:10.1083/jcb.148.5.1075
- Parsons, M., Messent, A. J., Humphries, J. D., Deakin, N. O. and Humphries, M. J. (2008). Quantification of integrin receptor agonism by fluorescence lifetime imaging. J. Cell Sci. 121, 265-271. doi:10.1242/jcs.018440
- Paulhe, F., Wehrle-Haller, M., Jacquier, M.-C., Imhof, B. A., Tabone-Eglinger, S. and Wehrle-Haller, B. (2009). Dimerization of Kit-ligand and efficient cell-surface presentation requires a conserved Ser-Gly-Gly-Tyr motif in its transmembrane domain. FASEB J. 23, 3037-3048. doi:10.1096/fj.09-129577
- Petrich, B. G., Fogelstrand, P., Partridge, A. W., Yousefi, N., Ablooglu, A. J., Shattil, S. J. and Ginsberg, M. H. (2007a). The antithrombotic potential of selective blockade of talin-dependent integrin alpha IIb beta 3 (platelet GPIIb-IIIa) activation. J. Clin. Invest. 117, 2250-2259. doi:10.1172/JCI31024
- Petrich, B. G., Marchese, P., Ruggeri, Z. M., Spiess, S., Weichert, R. A. M., Ye, F., Tiedt, R., Skoda, R. C., Monkley, S. J., Critchley, D. R. et al. (2007b). Talin is required for integrin-mediated platelet function in hemostasis and thrombosis. *J. Exp. Med.* 204, 3103-3111. doi:10.1084/jem.20071800
- Pinon, P., Pärssinen, J., Vazquez, P., Bachmann, M., Rahikainen, R., Jacquier, M.-C., Azizi, L., Määttä, J. A., Bastmeyer, M., Hytönen, V. P. et al. (2014). Talinbound NPLY motif recruits integrin-signaling adapters to regulate cell spreading and mechanosensing. J. Cell Biol. 205, 265-281. doi:10.1083/jcb.201308136
- Podleski, T. R., Greenberg, I., Schlessinger, J. and Yamada, K. M. (1979). Fibronectin delays the fusion of L6 myoblasts. Exp. Cell Res. 122, 317-326. doi:10.1016/0014-4827(79)90308-2
- Praekelt, U., Kopp, P. M., Rehm, K., Linder, S., Bate, N., Patel, B., Debrand, E., Manso, A. M., Ross, R. S., Conti, F. et al. (2012). New isoform-specific monoclonal antibodies reveal different sub-cellular localisations for talin1 and talin2. *Eur. J. Cell Biol.* **91**, 180-191. doi:10.1016/j.ejcb.2011.12.003
- Qiao, L., Gao, H., Zhang, T., Jing, L., Xiao, C., Xiao, Y., Luo, N., Zhu, H., Meng, W., Xu, H. et al. (2014). Snail modulates the assembly of fibronectin via alpha5

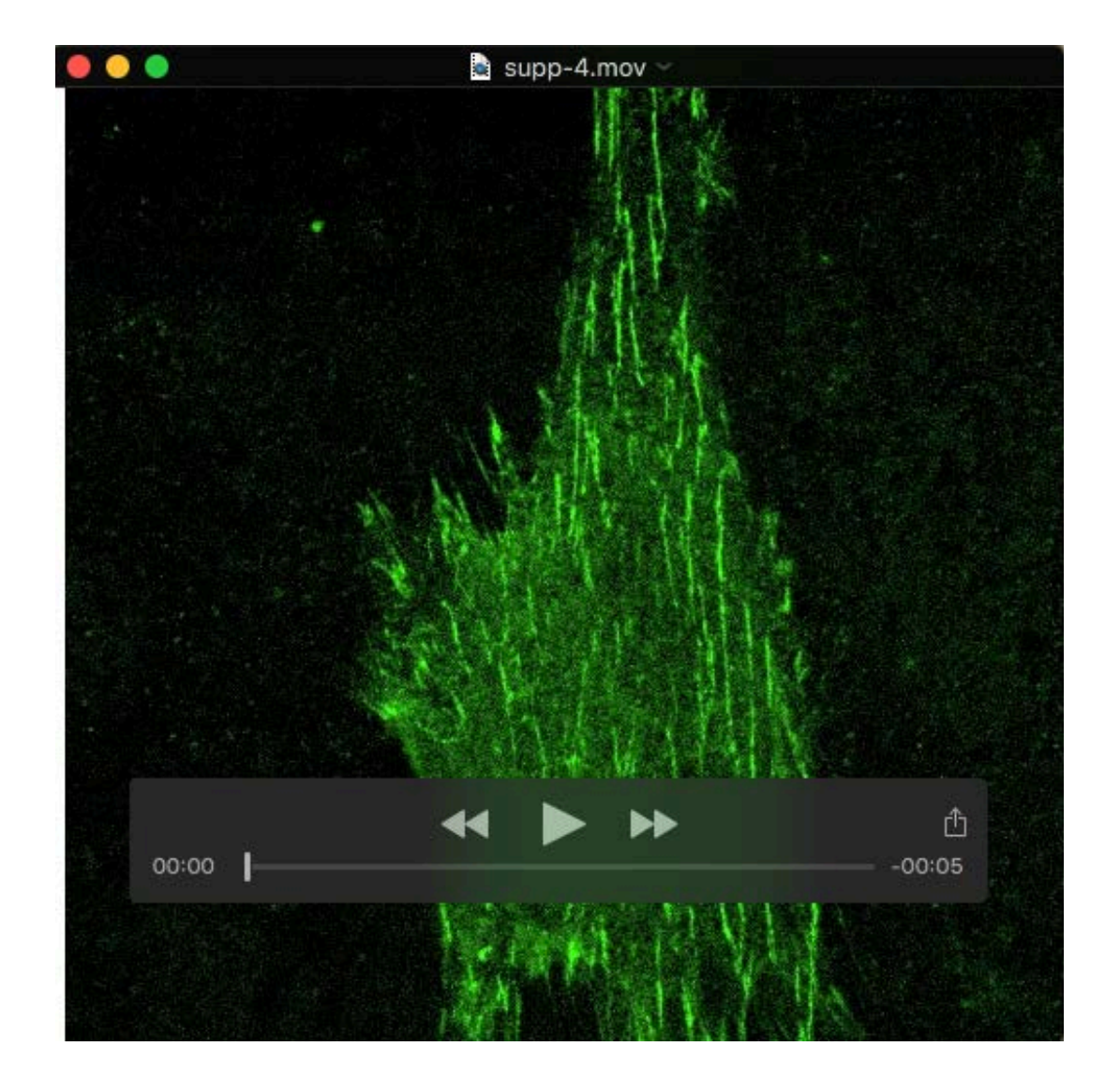
- integrin for myocardial migration in zebrafish embryos. *Sci. Rep.* **4**, 4470. doi:10. 1038/srep04470
- Rahikainen, R., von Essen, M., Schaefer, M., Qi, L., Azizi, L., Kelly, C., Ihalainen, T. O., Wehrle-Haller, B., Bastmeyer, M., Huang, C. et al. (2017). Mechanical stability of talin rod controls cell migration and substrate sensing. Sci. Rep. 7, 3571. doi:10.1038/s41598-017-03335-2
- Rozo, M., Li, L. and Fan, C.-M. (2016). Targeting beta1 integrin signaling enhances regeneration in aged and dystrophic muscle in mice. *Nat. Med.* 22, 889-896. doi:10.1038/nm.4116
- Sastry, S. K., Lakonishok, M., Wu, S., Truong, T. Q., Huttenlocher, A., Turner, C. E. and Horwitz, A. F. (1999). Quantitative changes in integrin and focal adhesion signaling regulate myoblast cell cycle withdrawal. *J. Cell Biol.* 144, 1295-1309. doi:10.1083/jcb.144.6.1295
- Schindelin, J., Rueden, C. T., Hiner, M. C. and Eliceiri, K. W. (2015). The ImageJ ecosystem: an open platform for biomedical image analysis. *Mol. Reprod. Dev.* 82, 518-529. doi:10.1002/mrd.22489
- Su, Y., Xia, W., Li, J., Walz, T., Humphries, M. J., Vestweber, D., Cabañas, C., Lu, C. and Springer, T. A. (2016). Relating conformation to function in integrin alpha5beta1. *Proc. Natl. Acad. Sci. USA* 113, E3872-E3881. doi:10.1073/pnas. 1605074113
- Suzuki, K. and Takahashi, K. (2003). Reduced cell adhesion during mitosis by threonine phosphorylation of beta1 integrin. *J. Cell. Physiol.* 197, 297-305. doi:10. 1002/jcp.10354
- Syed, A., Arora, N., Bunch, T. A. and Smith, E. A. (2016). The role of a conserved membrane proximal cysteine in altering alphaPS2CbetaPS integrin diffusion. *Phys. Biol.* **13**, 066005. doi:10.1088/1478-3975/13/6/066005
- Tabone-Eglinger, S., Wehrle-Haller, M., Aebischer, N., Jacquier, M.-C. and Wehrle-Haller, B. (2012). Membrane-bound Kit ligand regulates melanocyte adhesion and survival, providing physical interaction with an intraepithelial niche. *FASEB J.* 26, 3738-3753. doi:10.1096/fj.12-206045
- Tabone-Eglinger, S., Calderin-Sollet, Z., Pinon, P., Aebischer, N., Wehrle-Haller, M., Jacquier, M.-C., Boettiger, D. and Wehrle-Haller, B. (2014). Niche anchorage and signaling through membrane-bound Kit-ligand/c-kit receptor are kinase independent and imatinib insensitive. FASEB J. 28, 4441-4456. doi:10.1096/fj.14-249425
- Taverna, D., Disatnik, M.-H., Rayburn, H., Bronson, R. T., Yang, J., Rando, T. A. and Hynes, R. O. (1998). Dystrophic muscle in mice chimeric for expression of alpha5 integrin. J. Cell Biol. 143, 849-859. doi:10.1083/jcb.143.3.849
- Theodosiou, M., Widmaier, M., Böttcher, R. T., Rognoni, E., Veelders, M., Bharadwaj, M., Lambacher, A., Austen, K., Müller, D. J., Zent, R. et al. (2016). Kindlin-2 cooperates with talin to activate integrins and induces cell spreading by directly binding paxillin. eLife 5, e10130. doi:10.7554/eLife.10130
- Tseng, H.-Y., Thorausch, N., Ziegler, T., Meves, A., Fässler, R. and Böttcher, R. T. (2014). Sorting nexin 31 binds multiple beta integrin cytoplasmic domains and regulates beta1 integrin surface levels and stability. J. Mol. Biol. 426, 3180-3194. doi:10.1016/j.jmb.2014.07.003
- Tseng, H.-Y., Samarelli, A. V., Kammerer, P., Scholze, S., Ziegler, T., Immler, R., Zent, R., Sperandio, M., Sanders, C. R., et al. (2018). LCP1 preferentially binds clasped alphaMbeta2 integrin and attenuates leukocyte adhesion under flow. *J. Cell Sci.* 131, jcs218214. doi:10.1242/jcs.218214
- Tsunoyama, T. A., Watanabe, Y., Goto, J., Naito, K., Kasai, R. S., Suzuki, K. G. N., Fujiwara, T. K. and Kusumi, A. (2018). Super-long single-molecule tracking reveals dynamic-anchorage-induced integrin function. *Nat. Chem. Biol.* 14, 497-506. doi:10.1038/s41589-018-0032-5
- van der Flier, A., Kuikman, I., Baudoin, C., van der Neut, R. and Sonnenberg, A. (1995). A novel beta 1 integrin isoform produced by alternative splicing: unique expression in cardiac and skeletal muscle. FEBS Lett. 369, 340-344. doi:10.1016/0014-5793(95)00814-P
- van der Flier, A., Gaspar, A. C., Thorsteinsdóttir, S., Baudoin, C., Groeneveld, E., Mummery, C. L. and Sonnenberg, A. (1997). Spatial and temporal expression of the beta1D integrin during mouse development. *Dev. Dyn.* 210, 472-486. doi:10. 1002/(SICI)1097-0177(199712)210:4<472::AID-AJA10>3.0.CO;2-9
- Wegener, K. L., Partridge, A. W., Han, J., Pickford, A. R., Liddington, R. C., Ginsberg, M. H. and Campbell, I. D. (2007). Structural basis of integrin activation by talin. *Cell* 128, 171-182. doi:10.1016/j.cell.2006.10.048
- Wehrle-Haller, B. (2007). Analysis of integrin dynamics by fluorescence recovery after photobleaching. *Methods Mol. Biol.* 370, 173-201. doi:10.1007/978-1-59745-353-0 13
- Yates, L. A., Füzéry, A. K., Bonet, R., Campbell, I. D. and Gilbert, R. J. C. (2012). Biophysical analysis of Kindlin-3 reveals an elongated conformation and maps integrin binding to the membrane-distal beta-subunit NPXY motif. *J. Biol. Chem.* **287**, 37715-37731. doi:10.1074/jbc.M112.415208
- Zamir, E., Katz, M., Posen, Y., Erez, N., Yamada, K. M., Katz, B.-Z., Lin, S., Lin, D. C., Bershadsky, A., Kam, Z. et al. (2000). Dynamics and segregation of cell-matrix adhesions in cultured fibroblasts. *Nat. Cell Biol.* 2, 191-196. doi:10.1038/35008607
- Zhidkova, N. I., Belkin, A. M. and Mayne, R. (1995). Novel isoform of beta 1 integrin expressed in skeletal and cardiac muscle. *Biochem. Biophys. Res. Commun.* 214, 279-285. doi:10.1006/bbrc.1995.2285



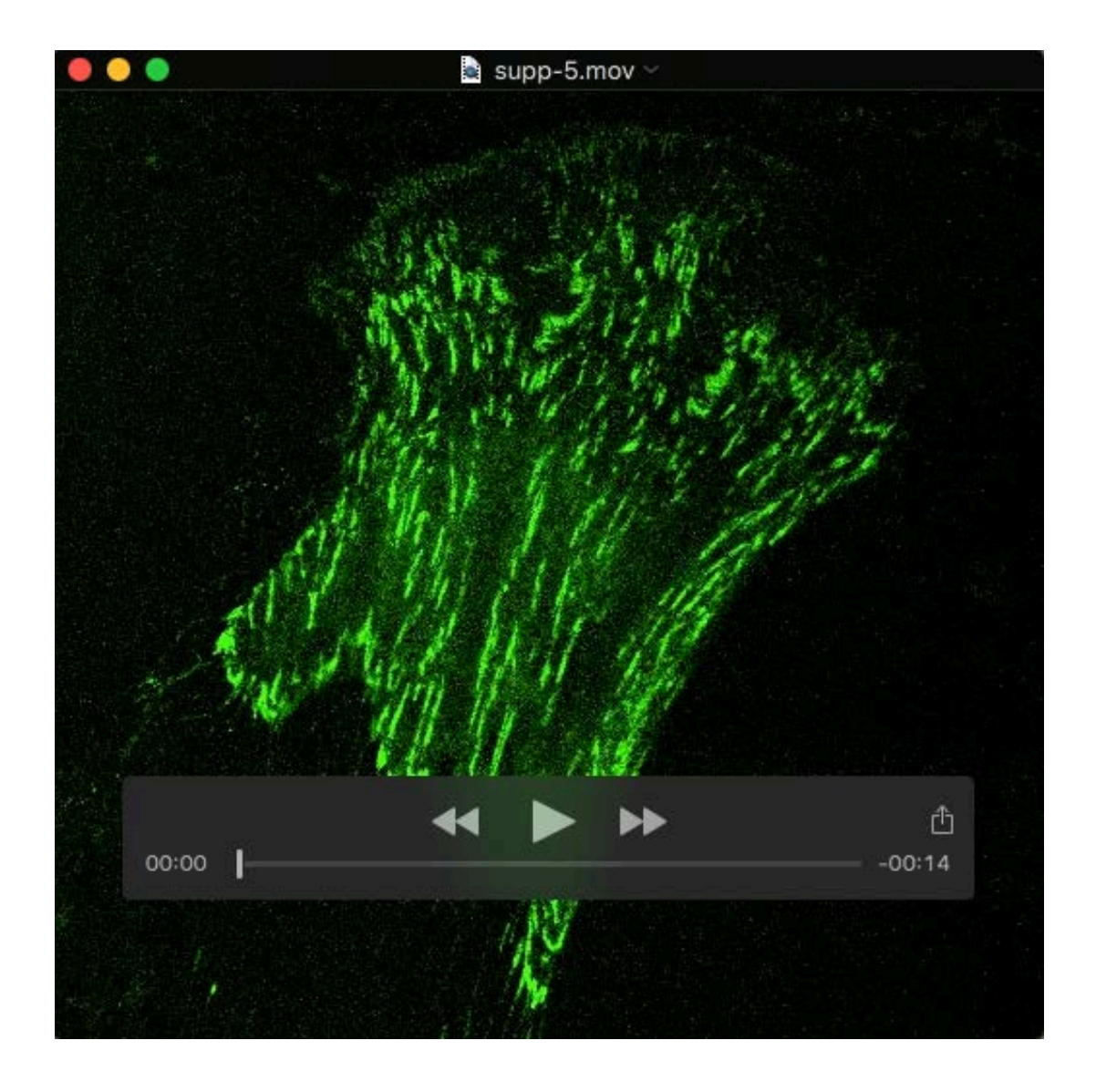
Movie 1 (.mov) to Fig. 1G (structural model of the extracellular tagged GFP- β 1-integrin fusion protein). The animation gives a 3D impression of the GFP-tagged (green) ligand-binding domain of α 5 β 1-integrin (RGD-peptide in yellow). Model based on the ligand-binding extracellular fragment of α 5 β 1 corresponding to 3VI4, and green fluorescent protein (GFP) corresponding to 1C4F.



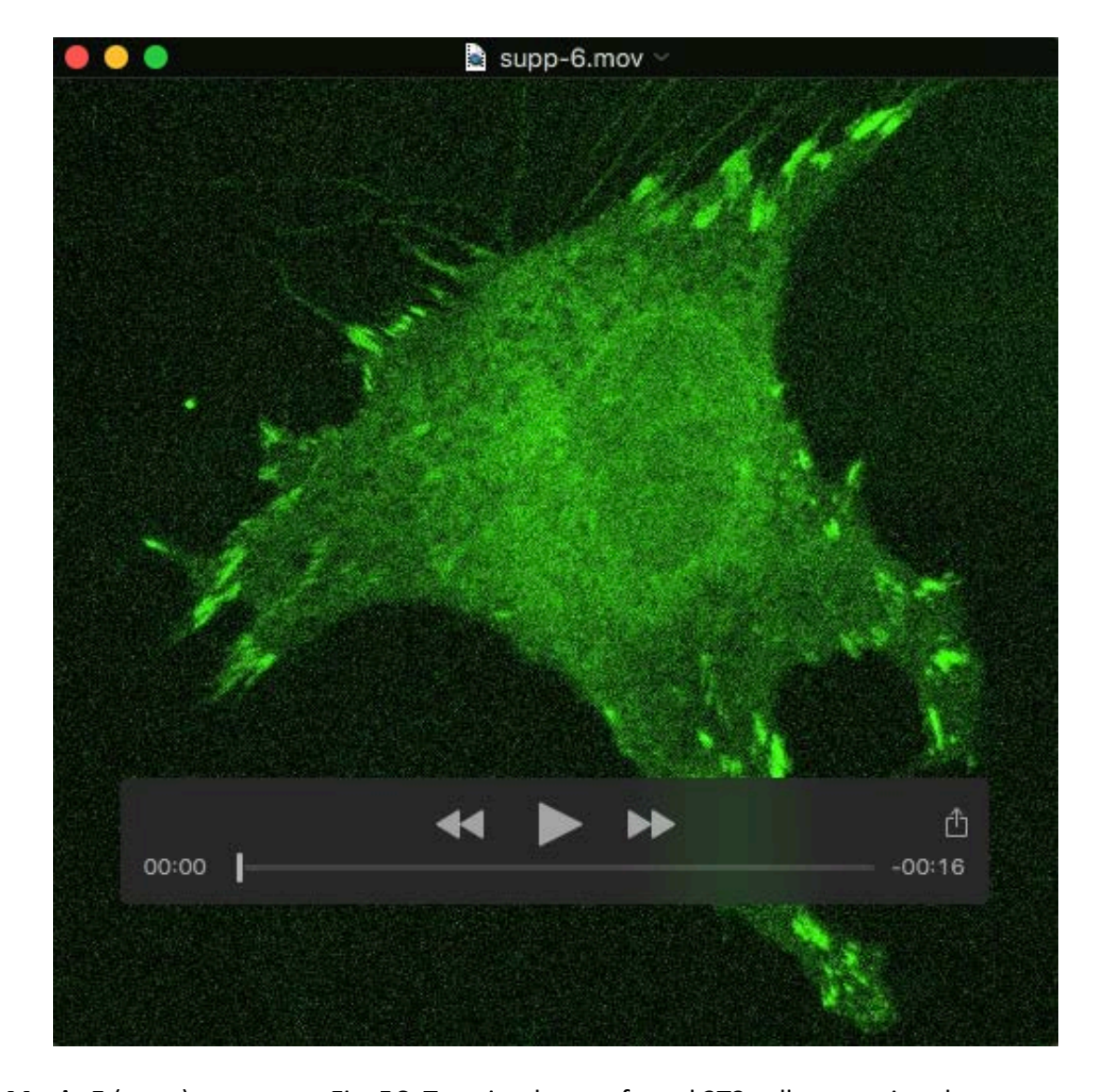
Movie 2 (.avi) to support Fig. 3D. C2C12 cell transiently expressing the GFP- β 1D-integrin construct for 72 hrs. Although the recovery of bleached GFP- β 1D-integrin structures on the surface of that cell is very slow, the individual GFP-positive fibers move on the surface of the cell (40 seconds between frames).



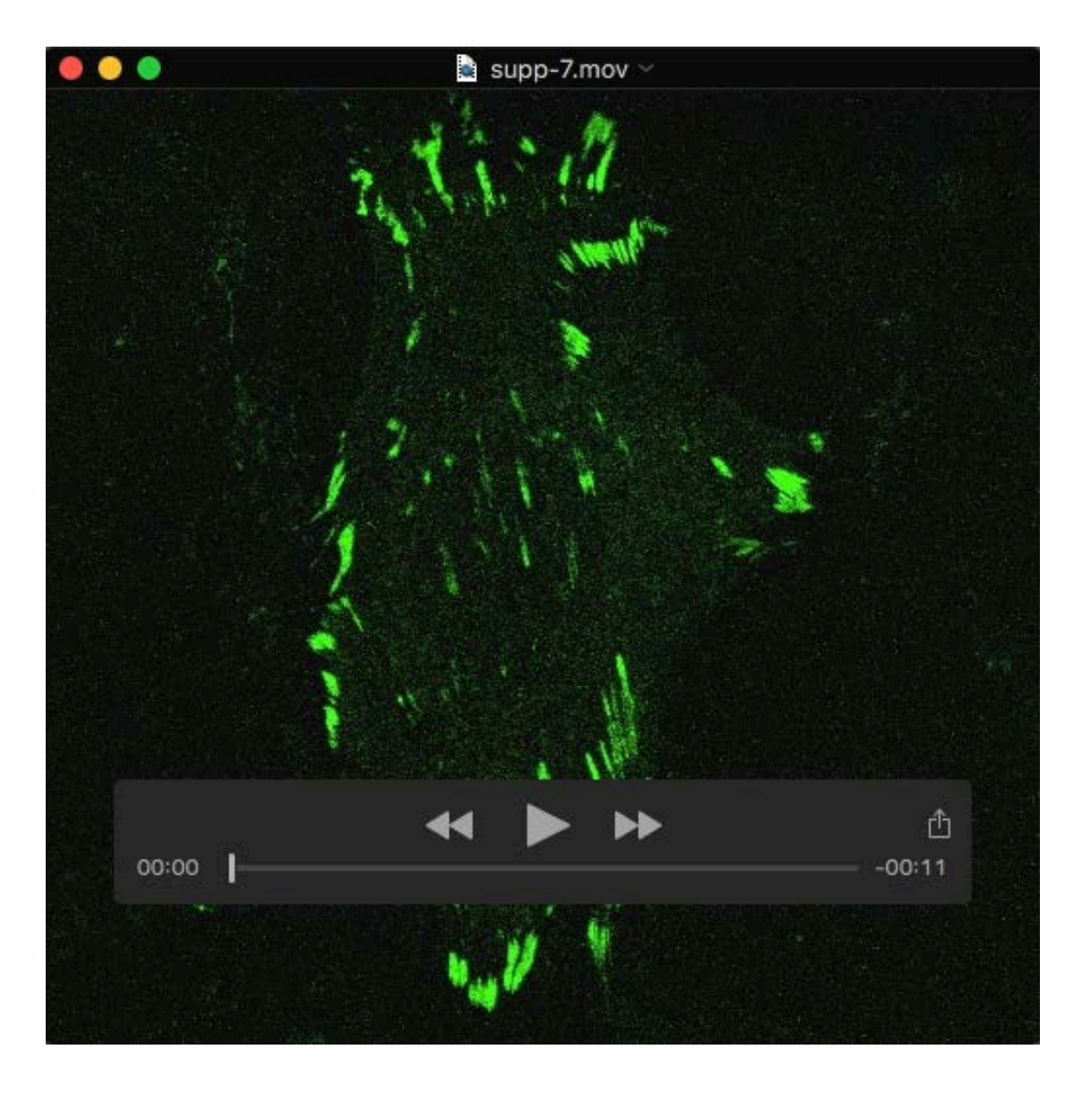
Movie 3 (.mov) to support Fig. 5A. Transiently transfected 3T3 cell expressing the GFP- β 1A-integrin construct for 72 hrs. Fluorescent structures are bleached and recovery can be observed over time (40 seconds between frames).



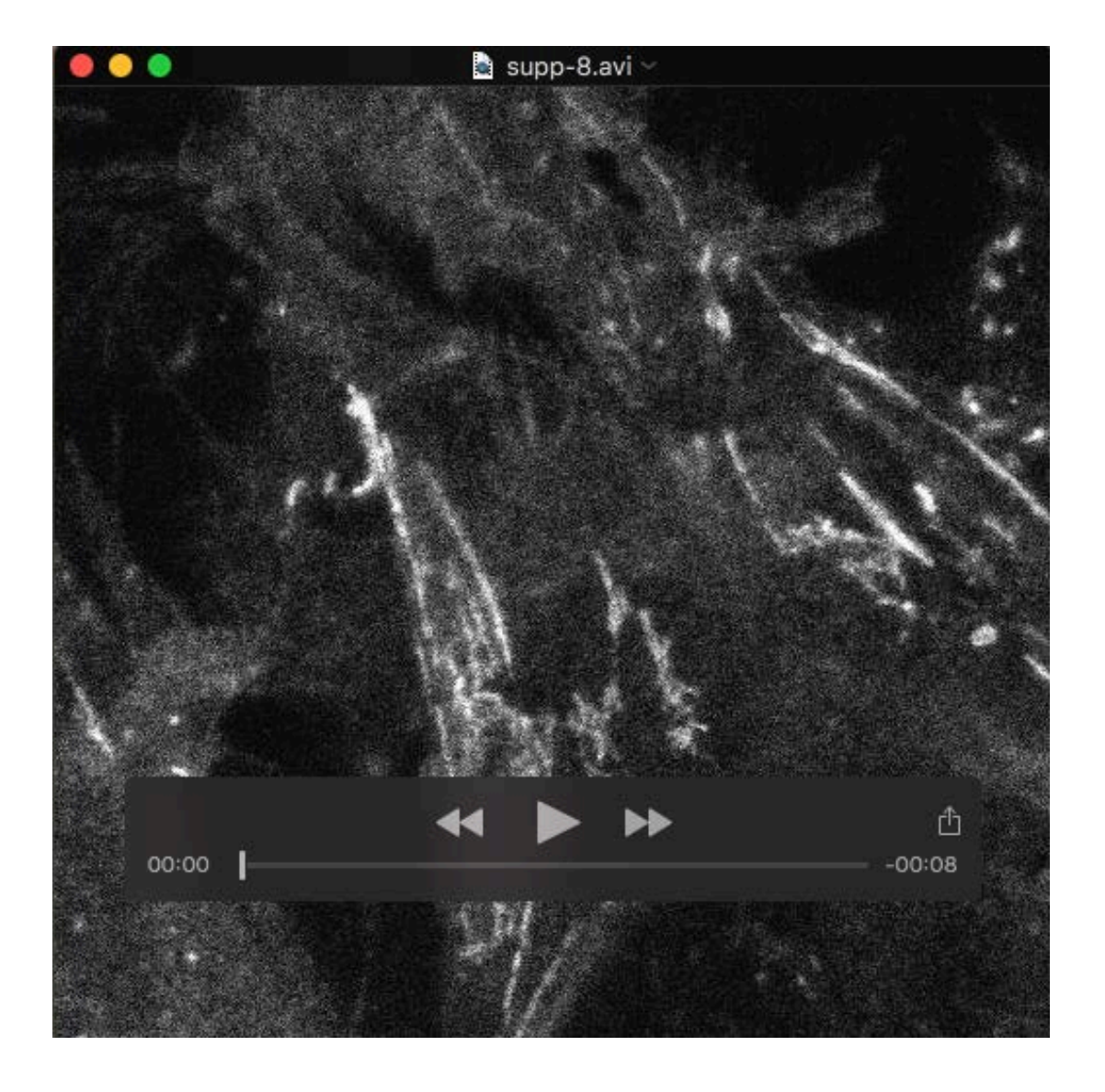
Movie 4 (.mov) to support Fig. 5B. Transiently transfected 3T3 cell expressing the GFP- β 1D-integrin construct for 72 hrs. Fluorescent structures are bleached and recovery can be observed over time (40 seconds between frames).



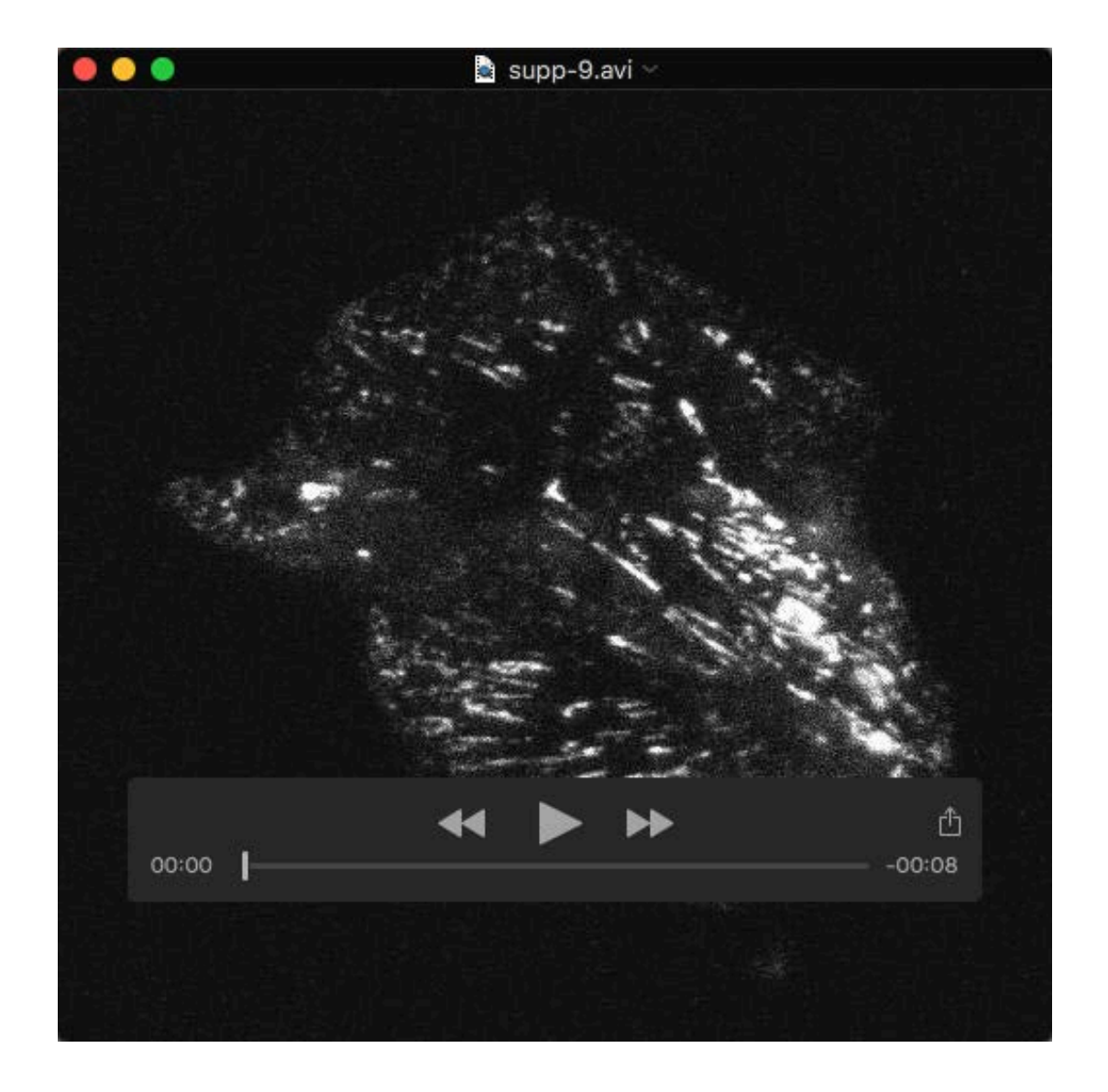
Movie 5 (.mov) to support Fig. 5C. Transiently transfected 3T3 cell expressing the GFP- β 1D-P786A-mutant-integrin construct for 72 hrs. Fluorescent structures are bleached and recovery can be observed over time (40 seconds between frames).



Movie 6 (.mov) to support Fig. 5D. Transiently transfected 3T3 cell expressing the β 3-GFP-integrin construct for 72 hrs. Fluorescent structures are bleached and recovery can be observed over time (40 seconds between frames).



Movie 7 (.avi) to support Fig. 5F. Representative example of a stably transfected GD25 cell expressing the GFP- β 1A-integrin construct. Fluorescent structures are bleached and recovery was followed over time to establish the data in Fig. 5F (20 seconds between frames. Width of field 53 μ m).



Movie 8 (.avi) to support Fig. 5F. Representative example of a stably transfected GD25 cell expressing the GFP- β 1D-integrin construct. Fluorescent structures are bleached and recovery was followed over time to establish the data in Fig. 5F (20 seconds between frames. Width of field 53 μ m).